

RESEARCH PAPER



Synthesis, potential antitumor activity, cell cycle analysis, and multitarget mechanisms of novel hydrazones incorporating a 4-methylsulfonylbenzene scaffold: a molecular docking study

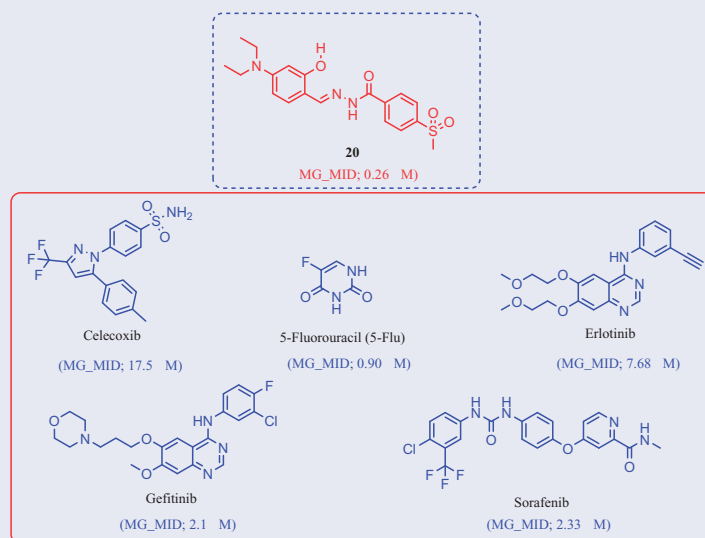
Alaa A.-M. Abdel-Aziz , Adel S. El-Azab , Nawaf A. AlSaif , Ahmad J. Obaidullah ,
Abdulrahman M. Al-Obaid and Ibrahim A. Al-Suwaidan

Department of Pharmaceutical Chemistry, College of Pharmacy, King Saud University, Riyadh Saudi Arabia

ABSTRACT

Hydrazone is a bioactive pharmacophore that can be used to design antitumor agents. We synthesised a series of hydrazones (compounds **4–24**) incorporating a 4-methylsulfonylbenzene scaffold and analysed their potential antitumor activity. Compounds **6**, **9**, **16**, and **20** had the most antitumor activity with a positive cytotoxic effect (PCE) of 52/59, 27/59, 59/59, and 59/59, respectively, while compounds **5**, **10**, **14**, **15**, **18**, and **19** had a moderate antitumor activity with a PCE of 11/59–14/59. Compound **20** was the most active and had a mean 50% cell growth inhibition (GI_{50}) of 0.26 μ M. Compounds **9** and **20** showed the highest inhibitory activity against COX-2, with a half-maximal inhibitory concentration (IC_{50}) of 2.97 and 6.94 μ M, respectively. Compounds **16** and **20** significantly inhibited EGFR (IC_{50} = 0.2 and 0.19 μ M, respectively) and HER2 (IC_{50} = 0.13 and 0.07 μ M, respectively). Molecular docking studies of derivatives **9**, **16**, and **20** into the binding sites of COX-2, EGFR, and HER2 were carried out to explore the interaction mode and the structural requirements for antitumor activity.

GRAPHICAL ABSTRACT






Compound **20** (MG_MID = 0.26 μ M) is nearly 65-fold more potent than celecoxib (MG_MID = 17.5 μ M), 3-fold more potent than 5-Fu (MG_MID = 0.90 μ M), 30-fold more potent than erlotinib (MG_MID = 7.68 μ M), and 9-fold more potent than gefitinib (MG_MID = 2.1 μ M) and sorafenib (MG_MID = 2.33 μ M).

1. Introduction

Cancer is the most dangerous disease and a leading cause of death worldwide¹. Also, cancer cells have evolved to become resistant to already used therapeutic agents^{2–4}. Therefore, novel and effective antitumor agents are in high demand, and their

development remains a challenge for pharmaceutical chemists^{5–21}. The use of more than one drug in combination with cancer therapy has several side effects^{22–24}. These effects can be diminished by using a single compound with multiple molecular mechanisms, which is currently the preferred therapeutic strategy^{25–30}. EGFR

CONTACT Alaa A.-M. Abdel-Aziz  almoenes@ksu.edu.sa  Department of Pharmaceutical Chemistry, College of Pharmacy, P.O. Box 2457, King Saud University, Riyadh 11451, Saudi Arabia

 Supplemental data for this article can be accessed [here](#).

© 2021 The Author(s). Published by Informa UK Limited, trading as Taylor & Francis Group.

This is an Open Access article distributed under the terms of the Creative Commons Attribution License (<http://creativecommons.org/licenses/by/4.0/>), which permits unrestricted use, distribution, and reproduction in any medium, provided the original work is properly cited.

and the structurally related human epidermal growth factor receptor 2 (HER2) are members of the tyrosine kinase receptor family^{31–35}. EGFR and HER2 overexpression has been found in various cancers, such as prostate, breast, colon, and ovarian cancers, and their inhibition results in apoptotic-inducing activity in lung and breast cancers^{36–39}. Therefore, EGFR and HER2 are important targets for antitumor agent design and development^{27,32,33,39–42}. Several tyrosine kinase inhibitors, such as imatinib (I), gefitinib (II), lapatinib (III), lapatinib (III), sorafenib (IV), afatinib (V), and sunitinib (VI), are used to treat various cancers (Figure 1)^{43–50}. In contrast, COX-2 isozyme is overexpressed in several cancers, such as colon, hepatocellular, gastric, breast, lung, prostate, and ovarian cancers, indicating that COX-2 is a target for cancer treatment^{51,52}. These findings show that celecoxib (VII) and other selective COX-2 inhibitors can be used for cancer treatment and prevention (Figure 2)^{53,54}. The anticancer mechanism through COX-2 inhibition might proceed *via* proliferation inhibition or apoptotic induction⁵⁵.

Hugo Schiff first prepared Schiff's bases or azomethines with an imine core skeleton (RHC=N-R) in 1864 through the reaction of carbonyl compounds and a primary amine⁵⁶. The chemical and

biological behaviours of Schiff's bases are due to the lone pair of electrons on the imine core, which are responsible for their chelating properties^{57,58}. Especially, hydrazone is an important, highly bioactive pharmacophore that can be used to design various anti-tumor agents, such as arylhydrazone (VIII), quinazolinyhydrazone (IX), and PAC-1 (X), and PAC-1 selectively induces apoptosis in cancer cells (Figure 2)^{21,59–63}. Other compounds with hydrazones show the tumour-associated carbonic anhydrase IX and COX-2 inhibition activities^{64–66}. Interestingly, compounds with methylsulfonylbenzene, such as vismodegib (XI), and hydrazine derivative--linked sulphonyl fragments, such as arylsulfonylhydrazone (XII), are potential antitumor agents against skin, hepatocellular, lung, and colon cancers and melanoma (Figure 2)^{66–69}. The mechanism underlying the anticancer activity of a few hydrazones has been investigated through selective COX-2 inhibition, EGFR, and HER2 inhibition, in addition to apoptosis induction^{39,60,66,69}.

In this study, we synthesised a series of hydrazones (compounds 4–24) incorporating a 4-methylsulfonylbenzene scaffold (Figure 3). The chemical structure of the designed compounds was based on some fragments of compounds shown in Figures 1

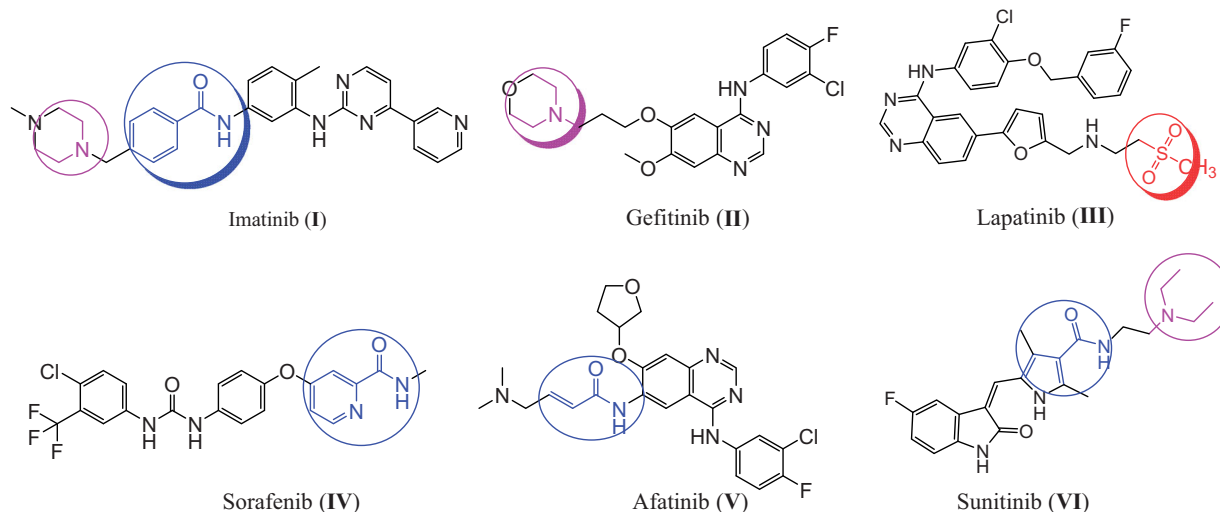


Figure 1. The reported anticancer agents with EGFR and HER2 inhibition activities.

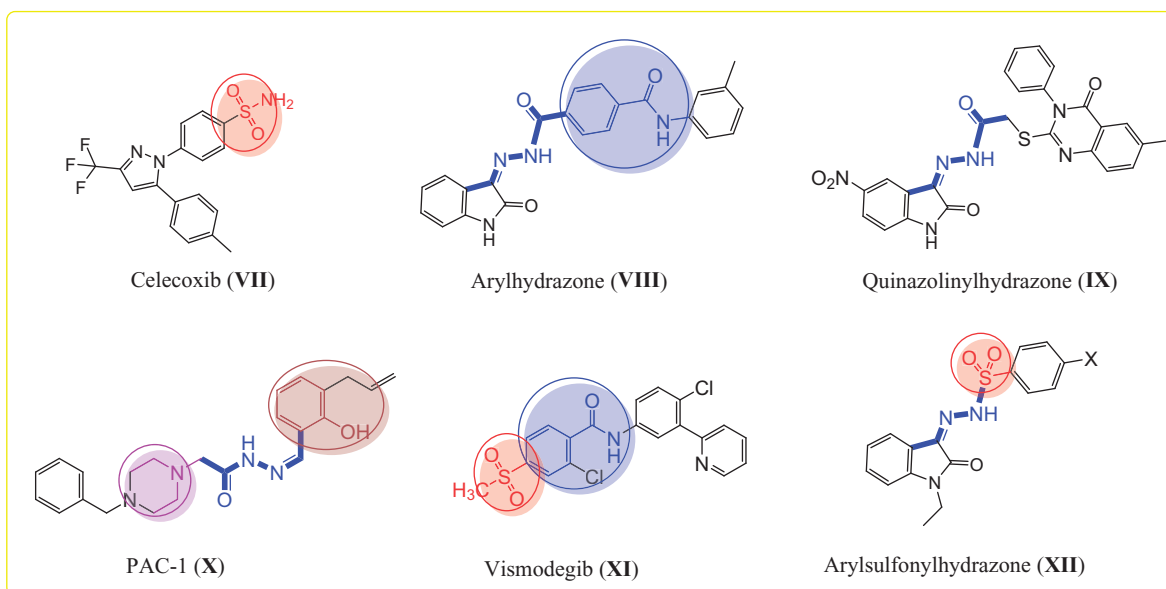


Figure 2. The reported anticancer agents bearing hydrazone, sulphonyl, and benzamide fragments.

and 2. A 4-methylsulfonylbenzene core was linked with a hydrazone moiety and connected with various arylidene with or without hydroxyl and *N,N*-diethylamine fragments (Figure 3). We also evaluated the *in vitro* antitumor activities of the synthesised compounds using 59 human cancer cell lines and investigated the structure–activity relationship (SAR) of the compounds with various substituents, depending on their antitumor activities. Next, we performed a cell cycle analysis and apoptotic induction assay of the most active compounds using the HL-60 cell line. We performed an enzymatic assay of the EGFR and HER2 inhibitory activity of the most promising compounds and evaluated the COX-2 inhibitory activity of the most active derivatives. Finally, we used molecular docking to predict the interaction mode of the biologically active compounds in the binding pockets of COX-2 isozyme, and EGFR, and HER2 tyrosine kinases.

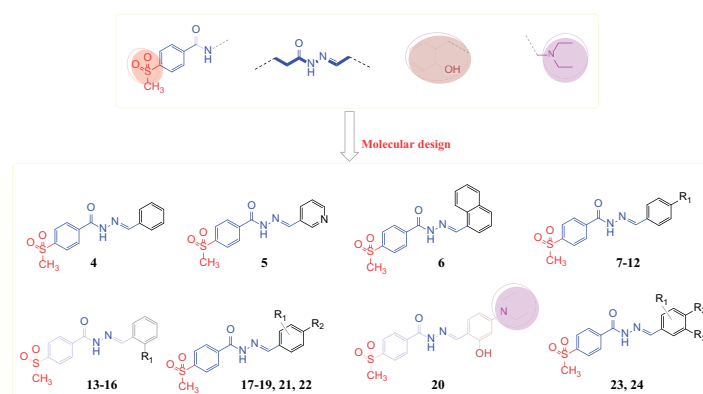


Figure 3. The designed target arylhydrazones 4–24 based on the chemical structure of compounds I–XII.

2. Results and discussion

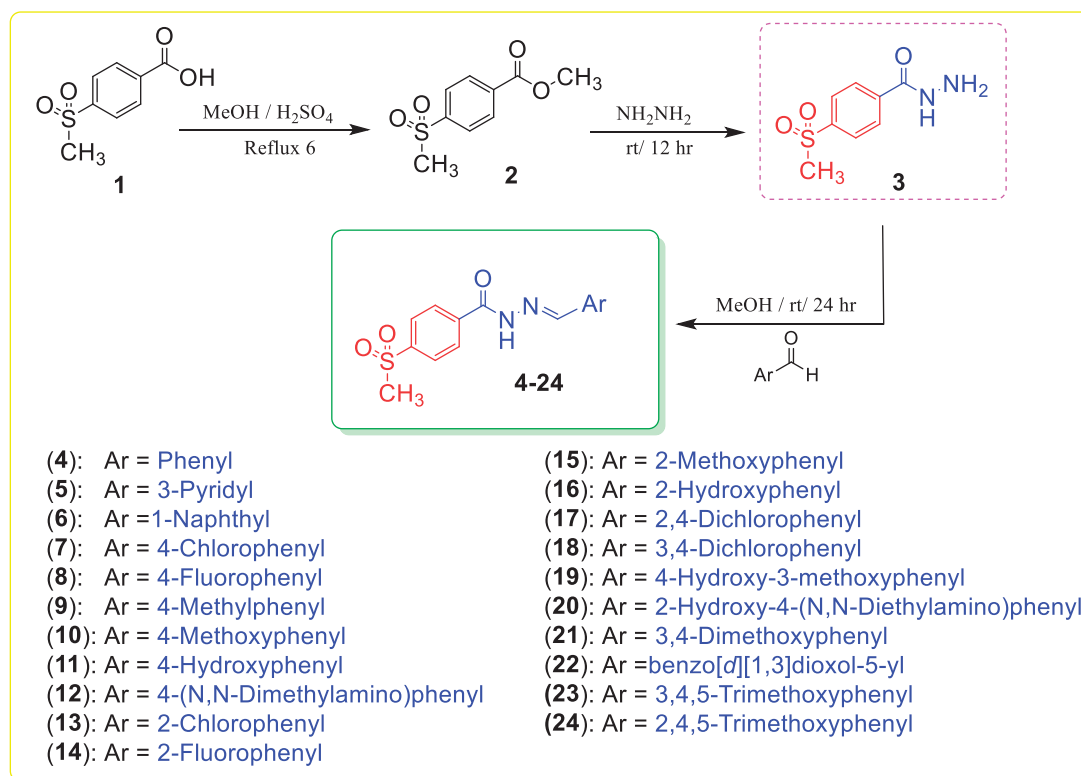
2.1. Chemistry

4-(Methylsulfonyl)-*N'*-(substituted-benzylidene)benzohydrazides 4–24 were obtained with a yield of 85–95% by stirring an appropriate aldehyde and 4-(methylsulfonyl)benzohydrazide (3) in methanol containing a catalytic amount of acetic acid at room temperature (Scheme 1). Multiple spectral analyses were performed to confirm the structures of target compounds 4–24. The amide fragment of the benzylidene benzohydrazide moiety (PhCONH=CHPh) was verified by ^1H NMR spectra with peaks at 12.35–11.81 ppm for the amidic proton and by ^{13}C NMR spectra with characteristic peaks at 163.0–161.3 ppm for the carbonyl group. In addition, the imine fragment of the benzylidene benzohydrazide moiety (PhCONH=CHPh) was verified by ^1H NMR spectra with peaks at 9.12–8.36 ppm and by ^{13}C NMR spectra with characteristic peaks at 151.4–143.9 ppm. The methyl group of the 4-methylsulfonyl moiety (SO_2CH_3) was verified by ^1H NMR and ^{13}C NMR spectra with peaks at 3.32–3.29 and 43.8–43.7 ppm, respectively.

2.2. Antitumor activity and SAR study

2.2.1. Growth inhibition percentage (GI) at a single dose concentration of 10 μM

Compounds 4–24 were selected by the National Cancer Institute (Bethesda, MD, USA) for evaluation of their *in vitro* antitumor activity against a full panel of 59 cancer cell lines (Tables 1 and 2) taken from nine human tissue (i.e. blood, lung, colon, brain, skin, ovary, kidney, prostate, and breast)^{17,40,70}. We performed the initial antitumor evaluation at a single dose concentration of 10 μM and calculated the GI in the 59 cell lines. The GI results were compared with those of imatinib, gefitinib, and 5-fluorouracil (5-FU) as reference drugs. Tables 1 and 2 summarise the GI activity of



Scheme 1. Synthesis of the designed hydrazones 4–24.

compounds **4–24**, which showed significant antitumor activity against the 59 cell lines at a 10 μM concentration with PCE (ratio between the number of cell lines with percentage growth inhibition from 10 to 100 and the total number of cell lines) of 5/59–59/59 and a percentage mean growth (MG) of 100.00%–20.59%. Compounds **5**, **6**, **9**, **10**, **14–16**, and **18–20** showed the highest PCE of 11/59–59/59 (MG = 99.74%–20.95%), while compounds **4**, **7**, **8**, **11–13**, **17**, and **21–24** showed the lowest PCE of $\leq 10/59$ (MG = 100.00%–95.96%) compared to imatinib (PCE = 20/55 and MG = 92.62%). Interestingly, compounds **6**, **9**, **16**, and **20** were the most active antitumor agents (PCE = 52/59, 27/59, 59/59, and 59/59, respectively, and MG = 71.75%, 88.01%, 39.27%, and 20.59%, respectively), while compounds **5**, **14**, **15**, **18**, and **19** showed moderate activity (PCE = 13/59, 12/59, 14/59, 14/59, and 13/59, respectively, and MG = 98.37%, 95.16%, 95.92%, 94.23%, and 96.65%, respectively).

Structure correlation analysis gave the following results:

- 2-hydroxyphenyl derivatives, such as compounds **16** and **20** (PCE = 59/59), had significant and potent antitumor activity compared to unsubstituted phenyl and 4-hydroxyphenyl derivatives, such as compounds **4**, **11**, and **19** (PCE = 10/59, 5/59, and 13/59, respectively).
- Derivatives incorporating the 2-hydroxyphenyl moiety, such as compounds **16** and **20** (PCE = 59/59), were potent antitumor agents compared to the corresponding 2-substituted compounds **13–15** (PCE = 10/59–14/59).
- Derivatives based on a naphthalene scaffold, such as compound **6**, showed a sharp increase in antitumor activity (PCE = 52/59) compared to phenyl and pyridyl compounds **4** and **5** (PCE = 10/59 and 13/59, respectively).
- Replacement of the phenyl moiety of compound **4** with a 4-tolyl fragment, such as in compound **9**, increased antitumor activity (PCE = 10/59 and 27/59, respectively).
- The 4-tolyl compound **9** showed significant antitumor activity (PCE = 27/59) compared to the corresponding halogenated derivatives, such as compounds **7** and **8** (PCE = 7/59 and 9/59, respectively), and derivatives incorporating 4-methoxyphenyl (compound **10**), 4-hydroxyphenyl (compound **11**), and 4-(*N,N*-dimethylamino)phenyl (compound **12**) fragments (PCE = 11/59, 5/59, and 9/59 respectively).
- Introduction of one or more methoxy group at the phenyl fragment, such as in compounds **10** and **21–24**, did not improve antitumor activity (PCE = 11/59, 8/59, 9/59, 9/59, and 8/59, respectively) compared to the unsubstituted phenyl compound **4** (PCE = 10/59).
- Insertion of a methoxy group into compound **11** (PCE = 5/59) at position three significantly increased the antitumor activity of compound **19** (PCE = 13/59).
- Insertion of a halogen atom into a phenyl derivative, such as compound **4** (PCE = 10/59), produced compounds **7**, **8**, **13**, and **14** with retention of antitumor activity (PCE = 7/59, 9/59, 10/59, and 12/59, respectively).
- Replacement of the 3,4-dimethoxyphenyl moiety, such as compound **21**, with a 3,4-dichlorophenyl derivative, such as compound **18**, increased antitumor activity (PCE = 8/59 and 14/59, respectively).

The broad-spectrum and selectivity of compounds **4–24** (Tables 1 and 2) against the 59 cell lines showed that compounds **6**, **9**, **16**, and **20** had significant GI (>10 –100%) against most of the cancer cell lines tested (leukaemia, non-small cell lung cancer [NSCLC], melanoma, and colon, CNS, ovarian, renal, prostate, and

breast cancer) compared to imatinib (GI < 10 –47.1%). Compounds **6**, **9**, **16**, and **20** showed significant antitumor activity against leukaemia (GI = 12.3–100%), NSCLC (GI = 10.4%–96.7%), colon cancer (GI = 13.9%–91.4%), CNS cancer (GI = 10.3%–96.0%), melanoma (GI = 10.6–100%), ovarian cancer (GI = 12.3%–83.2%), renal cancer (GI = 12.3–100%), prostate cancer (GI = 11.2%–75.5%), and breast cancer (GI = 12.4%–98.8%). In contrast, the antitumor activity of imatinib was moderate against leukaemia (GI = 12.6%–18.0%), NSCLC (GI = 10.6%–17.1%), colon cancer (GI = 11.5%–47.1%), CNS cancer (GI = 10.6%–24.5%), melanoma (GI = 11.6%–22.3%), ovarian cancer (GI < 10.0 %), renal cancer (GI < 10.0 %–13.7%), prostate cancer (GI = 10.6%–14.4%), and breast cancer (GI = 11.2%–29.1%).

2.2.2. *GI₅₀, TGI, and LC₅₀ of compound 20 and a comparative study*

Compound **20** was the most active broad-spectrum antitumor agent among the 21 compounds tested, so we evaluated its potencies (50% cell growth inhibition [GI₅₀]) in an advanced assay against a panel of 60 cancer cell lines (Figure S1 and Tables 3 and 4) at tenfold dilution of five different concentrations (100, 10, 1, 0.1, and 0.01 μM). We also comparatively compared the assay results to the potencies of celecoxib, erlotinib, gefitinib, sorafenib, vismodegib, and 5-Fu as reference drugs (Tables 3 and 4). Accordingly, we listed three dose–response parameters of antitumor activity for compound **20** and the reference drugs against each cell line in Table 4, including GI₅₀, total cell growth inhibition (TGI), and median lethal concentration (LC₅₀). In addition, we calculated the mean GI₅₀ graph midpoints (GI₅₀ MG_MID) for these parameters in order to obtain an average activity parameter over all cell lines for each molecule. Tables 3 and 4 list the GI₅₀ values, which show that compound **20** had significantly potent antitumor activity, with GI₅₀ = 0.063–11.7 μM . We compared this value to celecoxib, erlotinib, gefitinib, sorafenib, and vismodegib (GI₅₀ = 3.98–63.09, 0.10–100.0, 0.0125–10.0, 1.26–3.98, and 19.95–100.0 μM , respectively (Table 4). With regard to individual human organs, compound **20** showed significantly potent antitumor activity against leukaemia (mean GI₅₀ = 0.23 μM), NSCLC (mean GI₅₀ = 0.26 μM), colon cancer (mean GI₅₀ = 0.27 μM), CNS cancer (mean GI₅₀ = 0.22 μM), melanoma (mean GI₅₀ = 0.31 μM), ovarian cancer (mean GI₅₀ = 1.10 μM), renal cancer (mean GI₅₀ = 1.40 μM), prostate cancer (mean GI₅₀ = 0.23 μM), and breast cancer (mean GI₅₀ = 2.20 μM) (Tables 3 and 4). In contrast, celecoxib, 5-Fu, erlotinib, gefitinib, and sorafenib had the following mean GI₅₀: leukaemia (12.35, 2.82, 27.85, 2.56, and 1.91 μM , respectively), NSCLC (25.09, 13.59, 13.11, 2.05, and 2.34 μM , respectively), colon cancer (20.73, 0.27, 51.68, 5.23, and 2.19 μM , respectively), CNS cancer (17.22, 14.38, 16.99, 5.64, and 2.33 μM , respectively), melanoma (22.46, 7.83, 23.74, 3.68, and 1.87 μM , respectively), ovarian cancer (17.14, 5.17, 5.52, 3.05, and 2.89 μM , respectively), renal cancer (19.87, 0.93, 2.46, 1.41, and 2.86 μM , respectively), prostate cancer (14.22, 1.46, 20.90, 3.29, and 2.58 μM , respectively), and breast cancer (17.49, 6.87, 24.72, 4.67, and 2.17 μM , respectively) (Table 4). Comparing the antitumor activity of compound **20** with the reference drugs, we found that compound **20** (GI₅₀ MG_MID = 0.26 μM) is nearly 65-fold more potent than celecoxib (GI₅₀ MG_MID = 17.5 μM), 3-fold more potent than 5-Fu (GI₅₀ MG_MID = 0.90 μM), 30-fold more potent than erlotinib (GI₅₀ MG_MID = 7.68 μM), and 9-fold more potent than gefitinib (GI₅₀ MG_MID = 2.1 μM) and sorafenib (GI₅₀ MG_MID = 2.33 μM).

Table 1. Antitumor activity of the designed hydrazones at 10 μ M concentration.

Compd No	PCE ^b	60 cell lines assay in one dose 10.0 μ M concentration (GI%) ^a	
		Most sensitive cell lines	
4	10/59	<u>Leukaemia</u> (HL-60 (TB): 60.3, K-562: 11.3, MOLT-4: 25.5), <u>NSC Lung Cancer</u> (A549/ATCC: 28.5, HOP-62: 12.0, NCI-H522: 42.1), <u>CNS Cancer</u> (U251: 20.4), <u>Melanoma</u> (SK-MEL-2: 21.5, UACC-257: 44.2), <u>Ovarian Cancer</u> (OVCAR-8: 15.1).	
5	13/59	<u>Leukaemia</u> (CCRF-CEM: 11.1, HL-60(TB): 20.5, K-562: 18.8), <u>NSC Lung Cancer</u> (A549/ATCC: 10.6, HOP-62: 16.5, NCI-H226: 11.9, NCI-H522: 15.1), <u>Colon Cancer</u> (HT29: 13.3), <u>Ovarian Cancer</u> (SK-OV-3: 16.9), <u>Renal Cancer</u> (A498: 11.2, UO-31: 16.3), <u>Prostate Cancer</u> (PC-3: 17.9), <u>Breast Cancer</u> (T-47D: 13.7).	
6	52/59	<u>Leukaemia</u> (CCRF-CEM: 22.4, HL-60(TB): 62.5, K-562: 72.2, MOLT-4: 53.2, PRMI-8226: 12.3, SR: 67.5), <u>NSC Lung Cancer</u> (A549/ATCC: 58.7, EKVX: 12.6, HOP-62: 25.1, NCI-H226: 16.3, NCI-H23: 10.4, NCI-H460: 33.2, NCI-H522: 95.5), <u>Colon Cancer</u> (COLO 205: 14.3, HCC-2998: 15.5, HCT-116: 38.2, HCT-15: 50.2, HT29: 50.5, KM12: 49.2, SW-620: 63.8), <u>CNS Cancer</u> (SF-268: 14.3, SF-295: 24.0, SF-539: 10.7, SNB-19: 20.2, SNB-75: 10.3, U251: 23.7), <u>Melanoma</u> (LOX IMVI: 27.6, MALME-3M: 30.3, M14: 33.2, MDA-MB-435: 82.9, SK-MEL-2: 52.3, SK-MEL-28: 10.6, SK-MEL-5: 32.8, UACC-257: 58.9, UACC-62: 38.4), <u>Ovarian Cancer</u> (IGROV1: 36.8, OVCAR-3: 32.2, OVCAR-8: 16.2, NCI/ADR-RES: 26.5, SK-OV-3: 21.9), <u>Renal Cancer</u> (A498: 30.9, CAKI-1: 32.8, SN12C: 12.6, TK-10: 14.9, UO-31: 21.5), <u>Prostate Cancer</u> (PC-3: 21.2, DU-145: 11.2), <u>Breast Cancer</u> (MCF7: 55.1, HS 578 T: 14.9, BT-549: 12.4, T-47D: 14.7, MDA-MB-468: 25.8).	
7	7/59	<u>Leukaemia</u> (HL-60 (TB): 52.1, K-562: 14.0, MOLT-4: 29.4), <u>NSC Lung Cancer</u> (NCI-H522: 15.7), <u>Melanoma</u> (SK-MEL-2: 12.8), <u>Renal Cancer</u> (A498: 12.3), <u>Prostate Cancer</u> (PC-3: 22.8).	
8	9/59	<u>Leukaemia</u> (CCRF-CEM: 11.8, HL-60(TB): 23.1, K-562: 13.6, MOLT-4: 23.9, SR: 20.2), <u>NSC Lung Cancer</u> (A549/ATCC: 11.1, NCI-H522: 15.9), <u>Colon Cancer</u> (HCT-116: 10.8), <u>Melanoma</u> (UACC-257: 18.4).	
9	27/59	<u>Leukaemia</u> (CCRF-CEM: 20.8, HL-60(TB): 24.3, K-562: 44.1, MOLT-4: 22.6, SR: 43.8), <u>NSC Lung Cancer</u> (A549/ATCC: 12.7, NCI-H522: 53.9), <u>Colon Cancer</u> (HCT-116: 13.9, HCT-15: 16.3, HT29: 17.7, KM12: 25.1, SW-620: 15.2), <u>CNS Cancer</u> (U251: 13.7), <u>Melanoma</u> (MALME-3M: 15.2, MDA-MB-435: 47.5, SK-MEL-2: 19.8, SK-MEL-5: 13.5, UACC-257: 28.4, UACC-62: 19.1), <u>Ovarian Cancer</u> (IGROV1: 12.3, NCI/ADR-RES: 14.6), <u>Renal Cancer</u> (A498: 17.9, CAKI-1: 25.0, UO-31: 12.3), <u>Prostate Cancer</u> (PC-3: 26.9), <u>Breast Cancer</u> (MCF7: 21.4, MDA-MB-468: 21.5).	
10	11/59	<u>Leukaemia</u> (CCRF-CEM: 10.6, HL-60(TB): 42.9, MOLT-4: 21.1), <u>NSC Lung Cancer</u> (A549/ATCC: 29.8, NCI-H522: 13.4, NCI-H522: 20.8), <u>Colon Cancer</u> (HT29: 10.8), <u>Melanoma</u> (SK-MEL-2: 11.8, UACC-257: 29.0), <u>Ovarian Cancer</u> (OVCAR-8: 11.3), <u>Prostate Cancer</u> (PC-3: 13.8).	
11	5/59	<u>Leukaemia</u> (HL-60(TB): 50.5, K-562: 26.2, MOLT-4: 32.5), <u>NSC Lung Cancer</u> (NCI-H522: 11.7), <u>Prostate Cancer</u> (PC-3: 10.9).	
12	9/59	<u>Leukaemia</u> (HL-60(TB): 38.0, K-562: 17.2, MOLT-4: 29.8), <u>NSC Lung Cancer</u> (A549/ATCC: 28.4, HOP-62: 11.4, NCI-H522: 40.4), <u>Colon Cancer</u> (HT29: 20.5), <u>Melanoma</u> (UACC-257: 39.2), <u>Renal Cancer</u> (UO-31: 11.2).	
13	10/59	<u>Leukaemia</u> (HL-60(TB): 47.7, K-562: 32.5, MOLT-4: 32.3), <u>NSC Lung Cancer</u> (A549/ATCC: 21.6, HOP-62: 12.7), <u>CNS Cancer</u> (SNB-75: 15.1), <u>Melanoma</u> (UACC-257: 35.5), <u>Ovarian Cancer</u> (SK-OV-3: 11.7), <u>Renal Cancer</u> (UO-31: 15.7), <u>Breast Cancer</u> (T-47D: 12.5).	
14	12/59	<u>Leukaemia</u> (HL-60(TB): 36.0, K-562: 25.7, MOLT-4: 26.4, SR: 49.2), <u>NSC Lung Cancer</u> (A549/ATCC: 29.3, HOP-62: 15.8, NCI-H522: 26.0), <u>Colon Cancer</u> (HT29: 18.6), <u>Melanoma</u> (UACC-257: 42.4), <u>Ovarian Cancer</u> (OVCAR-8: 14.5), <u>Renal Cancer</u> (CAKI-1: 11.7), <u>Breast Cancer</u> (T-47D: 11.8).	
15	14/59	<u>Leukaemia</u> (CCRF-CEM: 16.1, HL-60(TB): 36.5, K-562: 23.4, MOLT-4: 11.6, SR: 15.6), <u>NSC Lung Cancer</u> (A549/ATCC: 11.9, HOP-62: 18.9, NCI-H226: 10.3), <u>Colon Cancer</u> (HCT-116: 10.7), <u>Melanoma</u> (UACC-257: 10.1), <u>Ovarian Cancer</u> (SK-OV-3: 17.1), <u>Renal Cancer</u> (UO-31: 14.4), <u>Prostate Cancer</u> (PC-3: 19.1), <u>Breast Cancer</u> (T-47D: 18.2).	
16	59/59	<u>Leukaemia</u> (CCRF-CEM: 84.7, HL-60(TB): 93.7, K-562: 59.5, MOLT-4: 90.8, PRMI-8226: 51.3, SR: 79.6), <u>NSC Lung Cancer</u> (A549/ATCC: 61.2, EKVX: 74.2, HOP-62: 71.8, NCI-H226: 44.8, NCI-H23: 45.2, NCI-H322M: 61.6, NCI-H460: 85.9, NCI-H522: 84.9), <u>Colon Cancer</u> (COLO 205: 68.8, HCC-2998: 52.7, HCT-116: 70.9, HCT-15: 82.0, HT29: 56.4, KM12: 65.9, SW-620: 56.7), <u>CNS Cancer</u> (SF-268: 61.6, SF-295: 62.0, SF-539: 44.7, SNB-19: 54.6, SNB-75: 22.3, U251: 72.2), <u>Melanoma</u> (LOX IMVI: 78.6, MALME-3M: 36.5, M14: 67.5, MDA-MB-435: 40.3, SK-MEL-2: 60.0, SK-MEL-28: 44.1, SK-MEL-5: 67.8, UACC-257: 77.4, UACC-62: 83.6), <u>Ovarian Cancer</u> (IGROV1: 59.0, OVCAR-3: 77.2, OVCAR-4: 56.3, OVCAR-5: 35.3, OVCAR-8: 72.1, NCI/ADR-RES: 70.1, SK-OV-3: 60.1), <u>Renal Cancer</u> (786-0: 67.0, A498: 24.8, ACHN: 71.7, CAKI-1: 65.1, RXF 393: 47.0, SN12C: 41.4, TK-10: 54.2, UO-31: 82.0), <u>Prostate Cancer</u> (PC-3: 45.7, DU-145: 59.6), <u>Breast Cancer</u> (MCF7: 77.5, MDA-MB-231/ATCC: 52.6, HS 578 T: 18.5, BT-549: 47.0, T-47D: 47.6, MDA-MB-468: 35.3).	
17	9/59	<u>NSC Lung Cancer</u> (A549/ATCC: 13.7, HOP-62: 10.2, NCI-H226: 13.6, NCI-H522: 25.0), <u>Colon Cancer</u> (HT29: 11.3), <u>CNS Cancer</u> (SNB-75: 10.9), <u>Melanoma</u> (UACC-257: 29.4), <u>Renal Cancer</u> (UO-31: 12.7), <u>Breast Cancer</u> (MDA-MB-468: 18.1).	
18	14/59	<u>Leukaemia</u> (HL-60(TB): 30.6, K-562: 17.7, MOLT-4: 31.7, SR: 24.5), <u>NSC Lung Cancer</u> (A549/ATCC: 20.1, NCI-H522: 17.2), <u>Colon Cancer</u> (HCT-116: 12.7), <u>Melanoma</u> (MALME-3M: 12.2, UACC-257: 21.8, UACC-62: 11.2), <u>Ovarian Cancer</u> (IGROV1: 15.0), <u>Renal Cancer</u> (A498: 16.0, CAKI-1: 10.1), <u>Prostate Cancer</u> (PC-3: 10.3).	
19	13/59	<u>Leukaemia</u> (HL-60(TB): 67.3, K-562: 27.2, MOLT-4: 30.9, SR: 18.5), <u>NSC Lung Cancer</u> (A549/ATCC: 29.3, HOP-62: 12.1, NCI-H522: 37.7), <u>Colon Cancer</u> (HT29: 17.5), <u>CNS Cancer</u> (U251: 13.0), <u>Melanoma</u> (SK-MEL-2: 13.9, UACC-257: 48.4), <u>Ovarian Cancer</u> (OVCAR-8: 19.6), <u>Renal Cancer</u> (UO-31: 12.8).	
20	59/59	<u>Leukaemia</u> (CCRF-CEM: 93.1, HL-60(TB): 100, K-562: 87.6, MOLT-4: 97.3, PRMI-8226: 79.0, SR: 91.0), <u>NSC Lung Cancer</u> (A549/ATCC: 87.5, EKVX: 84.5, HOP-62: 87.1, NCI-H226: 77.4, NCI-H23: 67.2, NCI-H322M: 75.0, NCI-H460: 96.7, NCI-H522: 90.1), <u>Colon Cancer</u> (COLO 205: 91.4, HCC-2998: 60.4, HCT-116: 81.6, HCT-15: 71.5, HT29: 78.2, KM12: 74.1, SW-620: 67.0), <u>CNS Cancer</u> (SF-268: 78.2, SF-295: 78.6, SF-539: 96.0, SNB-19: 68.0, SNB-75: 44.8, U251: 79.4), <u>Melanoma</u> (LOX IMVI: 90.3, MALME-3M: 86.0, M14: 96.6, MDA-MB-435: 62.8, SK-MEL-2: 80.5, SK-MEL-28: 72.88, SK-MEL-5: 100, UACC-257: 100, UACC-62: >100), <u>Ovarian Cancer</u> (IGROV1: 78.8, OVCAR-3: 66.6, OVCAR-4: 65.3, OVCAR-5: 67.5, OVCAR-8: 83.2, NCI/ADR-RES: 82.2, SK-OV-3: 61.0), <u>Renal Cancer</u> (786-0: 84.6, A498: 54.7, ACHN: 82.9, CAKI-1: 79.6, RXF 393: 71.5, SN12C: 68.8, TK-10: 69.5, UO-31: 100), <u>Prostate Cancer</u> (PC-3: 50.8, DU-145: 75.5), <u>Breast Cancer</u> (MCF7: 91.2, MDA-MB-231/ATCC: 56.8, HS 578 T: 32.0, BT-549: 69.3, T-47D: 70.0, MDA-MB-468: 98.8).	
21	8/59	<u>Leukaemia</u> (HL-60(TB): 45.9, K-562: 19.1, MOLT-4: 34.1), <u>NSC Lung Cancer</u> (NCI-H522: 15.7), <u>Colon Cancer</u> (HCT-116: 11.0), <u>CNS Cancer</u> (SNB-75: 14.2), <u>Renal Cancer</u> (CAKI-1: 11.0), <u>Prostate Cancer</u> (PC-3: 11.5).	
22	9/59	<u>Leukaemia</u> (CCRF-CEM: 13.0, HL-60(TB): 43.0, K-562: 14.5, MOLT-4: 29.9), <u>NSC Lung Cancer</u> (A549/ATCC: 32.3, NCI-H522: 14.0), <u>Colon Cancer</u> (HT29: 11.0), <u>Melanoma</u> (SK-MEL-2: 10.9, UACC-257: 40.9).	
23	9/59	<u>Leukaemia</u> (HL-60(TB): 44.2, K-562: 37.6, MOLT-4: 32.6), <u>NSC Lung Cancer</u> (A549/ATCC: 22.8), <u>Colon Cancer</u> (COLO 205: 14.6), <u>CNS Cancer</u> (SNB-75: 11.3), <u>Melanoma</u> (UACC-257: 28.6), <u>Ovarian Cancer</u> (SK-OV-3: 14.2), <u>Renal Cancer</u> (UO-31: 10.2).	
24	8/59	<u>Leukaemia</u> (MOLT-4: 21.4), <u>NSC Lung Cancer</u> (A549/ATCC: 17.1, NCI-H522: 39.8), <u>Colon Cancer</u> (HT29: 17.9), <u>Melanoma</u> (K-MEL-2: 11.7, UACC-257: 21.6), <u>Renal Cancer</u> (UO-31: 10.5), <u>Prostate Cancer</u> (PC-3: 18.6).	
Imatinib	20/54	<u>Leukaemia</u> (MOLT-4: 18.0, PRMI-8226: 12.6, SR: 14.6), <u>NSC Lung Cancer</u> (EKVX: 15.7, NCI-H226: 10.6, NCI-H23: 17.1), <u>Colon Cancer</u> (HCT-116: 18.6, HCT-15: 11.5, HT29: 47.1), <u>CNS Cancer</u> (SF-295: 15.1, SF-539: 24.5, U251: 10.6), <u>Melanoma</u> (LOX IMVI: 11.6, SK-MEL-5: 22.3), <u>Renal Cancer</u> (A498: 13.7), <u>Prostate Cancer</u> (PC-3: 10.6, DU-145: 14.4), <u>Breast Cancer</u> (MDA-MB-231/ATCC: 11.2, T-47D: 18.6, MDA-MB-468: 29.1).	

^aGrowth Inhibition percentages (GI%) lower than 10% are not shown.^bPCE: Positive cytotoxic effect (ratio between the number of cell lines with percentage growth inhibition from 10 to 100 and the total number of cell lines).

Table 2. Growth inhibition percentage (GI%) of the most active hydrazones against individual cell lines.

Growth inhibition percentage (GI%)							
Subpanel tumour cell lines	6	9	16	20	Imatinib	Gefitinib	5-Fu
Leukaemia							
CCRF-CEM	22.4	20.8	84.7	93.1	–	96.0	42.9
HL-60(TB)	62.5	24.3	93.7	>100	–	100	52.1
K-562	72.2	44.1	59.5	87.6	NT	NT	57.7
MOLT-4	53.2	22.6	90.8	97.3	18.0	>100	56.9
PRMI-8226	12.3	–	51.3	79.0	12.6	18.0	58.6
SR	67.5	43.8	79.6	91.0	14.6	44.7	75.2
Non-Small Cell Lung Cancer							
A549/ATCC	58.7	12.7	61.2	87.5	–	87.0	65.8
EKVX	12.6	–	74.2	84.5	15.7	92.3	41.6
HOP-62	25.1	–	71.8	87.1	NT	NT	52.2
NCI-H226	16.3	–	44.8	77.4	10.6	25.2	30.5
NCI-H23	10.4	–	45.2	67.2	17.1	86.2	61.0
NCI-H322M	–	–	61.6	75.0	NT	NT	40.5
NCI-H460	33.2	–	85.9	96.7	–	42.7	87.0
NCI-H522	95.5	53.9	84.9	90.1	NT	NT	42.0
Colon Cancer							
COLO 205	14.3	–	68.8	91.4	–	49.6	59.8
HCC-2998	15.5	–	52.7	60.4	–	55.3	>100
HCT-116	38.2	13.9	70.9	81.6	18.6	72.1	82.2
HCT-15	50.2	16.3	82.0	71.5	11.5	71.5	73.5
HT29	50.5	17.7	56.4	78.2	47.1	50.3	72.9
KM12	49.2	25.1	65.9	74.1	–	36.9	59.3
SW-620	63.8	15.2	56.7	67.0	–	29.3	49.9
CNS Cancer							
SF-268	14.3	–	61.6	78.2	–	64.1	41.0
SF-295	24.0	–	62.0	78.6	15.1	15.8	30.9
SF-539	10.7	–	44.7	96.0	24.5	15.1	>100
SNB-19	20.2	–	54.6	68.0	–	73.8	34.1
SNB-75	10.3	–	22.3	44.8	–	61.5	34.1
U251	23.7	13.7	72.2	79.4	10.6	56.5	49.7
Melanoma							
LOX IMVI	27.6	–	78.6	90.3	11.6	46.0	69.6
MALME-3M	30.3	15.2	36.5	86.0	–	22.1	41.8
M14	33.2	–	67.5	96.6	–	89.7	NT
MDA-MB-435	82.9	47.5	40.3	62.8	–	63.3	63.4
SK-MEL-2	52.3	19.8	60.0	80.5	NT	NT	–
SK-MEL-28	10.6	–	44.1	72.8	–	27.3	NT
SK-MEL-5	32.8	13.5	67.8	>100	22.3	58.1	66.3
UACC-257	58.9	28.4	77.4	>100	–	24.7	80.5
UACC-62	38.4	19.1	83.6	>100	–	28.3	60.3
Ovarian Cancer							
IGROV1	36.8	12.3	59.0	78.8	–	57.2	48.8
OVCAR-3	32.2	–	77.2	66.6	–	55.8	52.6
OVCAR-4	–	–	56.3	65.3	–	11.5	40.6
OVCAR-5	–	–	35.3	67.5	–	54.5	55.7
OVCAR-8	16.2	–	72.1	83.2	–	78.2	NT
NCI/ADR-RES	26.5	14.6	70.1	82.2	–	86.3	52.4
SK-OV-3	21.9	–	60.1	61.0	–	83.0	22.5
Renal Cancer							
786-0	–	–	67.0	84.6	–	80.7	51.3
A498	30.9	17.9	24.8	54.7	13.7	65.9	>100
ACHN	–	–	71.7	82.9	–	91.5	60.7
CAKI-1	32.8	25.0	65.1	79.6	–	98.8	60.6
RXF 393	–	–	47.0	71.5	–	36.0	65.7
SN12C	12.6	–	41.4	68.8	–	85.5	46.0
TK-10	14.9	–	54.2	69.5	–	75.0	33.1
UO-31	21.5	12.3	82.0	>100	–	89.7	58.7
Prostate Cancer							
PC-3	21.2	26.9	45.7	50.8	10.6	49.6	41.8
DU-145	11.2	–	59.6	75.5	14.4	69.6	64.5
Breast Cancer							
MCF7	55.1	21.4	77.5	91.2	–	56.0	88.5
MDA-MB-231/ATCC	–	–	52.6	56.8	11.2	31.4	21.9
HS 578 T	14.9	–	18.5	32.0	–	10.0	>100
BT-549	12.4	–	47.0	69.3	–	61.2	62.2
T-47D	14.7	–	47.6	70.0	18.6	26.8	43.3
MDA-MB-468	25.8	21.5	35.3	98.8	29.1	>100	NT

NT: Not tested.

2.3. Apoptosis assay

2.3.1. Annexin V-FITC apoptosis assay

Apoptosis induction is the most important mechanism by which major chemotherapeutics kill cancer cells⁷¹. Apoptosis causes cellular changes whereby the translocation of phosphatidylserine (PS) occurs through the plasma membrane from the inside to the outside⁷¹. Annexin-V can bind to PS, which can be used as a sensitive probe for PS on the outer side of the plasma membrane⁷². We performed cytometric analysis to distinguish apoptosis from the necrosis mode of HL60 cell death induced by the most active compounds **6**, **9**, **16**, and **20** using annexin V-fluorescein isothiocyanate (FITC)/propidium iodide (AV/PI) dual-staining assay with the BD FACSCalibur (BD Biosciences, San Jose, CA, USA) (Table 5). The AV/PI staining of HL60 cells was performed at a mixed molar concentration of 10 μ M with compounds **6**, **9**, **16**, and **20** for 24 h. Figure 4 and Table 5 show the results of treating HL60 cells with compounds **6**, **9**, **16**, and **20** for 24 h. We found an increase in the early apoptosis ratio (Figure 4, lower-right quadrant of the cytogram) from 0.57% in the control sample (DMSO) to 3.52%–8.42% and a sharp increase in the late apoptosis ratio (Figure 4, upper-right quadrant of the cytogram) from 0.22% to 7.64%–13.41%. These data support the apoptotic mechanism underlying programmed cell death induced by compounds **6**, **9**, **16**, and **20** rather than the necrotic pathway.

2.3.2. In vitro cell cycle analysis

Antitumor agents can induce apoptosis by activating signalling pathways, leading to G2/M phase arrest^{73,74}. Flow cytometry is used to measure cell growth in different cell cycle phases (pre-G1, G1, S, and G2/M)^{73,74}. We selected the most active compounds **6**, **9**, **16**, and **20** for further analysis of their effects on cell cycle progression in the HL60 cell line (Figure 5 and Table 6). We used the solvent DMSO as a negative control. Briefly, we incubated HL60 cells with 10 μ M compounds **6**, **9**, **16**, and **20** for 24 h. Compounds **6**, **9**, **16**, and **20** interfered with the normal cell cycle of HL60 cells. There was a significant effect on the percentage of apoptotic cells, as indicated by an increase in cells in the pre-G1 phase (12.57%–24.31%) and the G2/M phase (23.27%–38.09%) compared to the control (1.71% and 12.03% cells, respectively). In contrast, the percentage of cells in S and G0/G1 phases significantly decreased (22.49%–29.43% and 36.28%–48.31%, respectively) compared to the control (35.3% and 52.67%, respectively), causing cell cycle arrest. These results clearly indicated that compounds **6**, **9**, **16**, and **20** arrests the G2/M phase of the cell cycle (Figure 5 and Table 6).

2.4. Enzymatic inhibition assay

2.4.1. Cox-2 inhibition activity

COX-2 is overexpressed in several cancer cell lines during cell proliferation. Its inhibition is used as a target for cancer treatment and prevention^{51,52,75}. Therefore, we performed COX-2 inhibition assays (kit catalogue no. 560101; Cayman Chemicals Inc., Ann Arbor, MI, USA) using compounds **6**, **9**, **16**, and **20**, which showed the highest antitumor activity, in addition to the reference drug celecoxib^{15,76}. The results were expressed as IC₅₀ (μ M) as the mean of three acquired determinations (Table 7). The IC₅₀ of celecoxib as a COX-2 inhibitor was 2.79 μ M. Compounds **9** and **20** were the most active COX-2 inhibitors (IC₅₀ = 2.97 and 6.94 μ M, respectively). In contrast, compounds **6** and **16** showed significantly low COX-2 inhibition (IC₅₀ = 36.27 and 82.45 μ M, respectively). Compounds with the 4-

Table 3. Influence of compound 20, and reference drugs on the growth of the individual tumour cell lines; median growth inhibitory (GI_{50} , μ M).

Subpanel tumour cell lines	GI_{50} (μ M)					
	20 (799156/1) ^a	Celecoxib (719627) ^a	Erlotinib (718781) ^a	Gefitinib (759856) ^a	Sorafenib (747971) ^a	Vismodegib (755986) ^a
<i>Leukaemia</i>						
CCRF-CEM	0.078	12.58	50.12	0.398	1.99	31.62
HL-60(TB)	0.164	15.85	25.12	1.0	1.58	31.62
K-562	0.604	10.00	31.62	2.51	3.16	31.62
MOLT-4	0.164	15.85	25.12	1.995	3.16	31.62
PRMI-8226	0.297	3.98	25.12	6.31	1.58	31.62
SR	0.063	15.85	10.00	3.16	3.16	39.81
<i>Non-Small Cell Lung Cancer</i>						
A549/ATCC	0.402	15.85	10.00	2.51	3.16	39.81
EKVX	0.162	19.95	0.199	0.0501	2.51	39.81
HOP-62	0.085	63.09	15.85	3.16	1.99	79.43
HOP-92	0.491	NT ^b	3.98	0.316	1.58	25.12
NCI-H226	0.073	NT ^b	39.81	3.98	1.99	50.12
NCI-H23	0.446	15.85	31.62	2.51	1.99	50.12
NCI-H322M	0.228	19.95	0.10	0.063	2.51	100
NCI-H460	0.113	15.85	6.31	3.16	2.51	39.81
NCI-H522	0.395	NT ^b	1.00	1.0	1.99	25.12
<i>Colon Cancer</i>						
COLO 205	0.269	15.85	50.12	7.94	1.99	39.81
HCC-2998	0.301	15.85	79.43	2.51	3.16	39.81
HCT-116	0.121	50.01	6.31	3.16	1.58	50.12
HCT-15	0.092	15.85	3.98	3.98	2.51	31.62
HT29	0.297	15.85	63.09	3.98	1.99	25.12
KM12	0.404	15.85	79.43	10.0	1.58	31.62
SW-620	0.387	15.85	79.43	5.011	2.51	63.09
<i>CNS Cancer</i>						
SF-268	0.0789	15.85	15.84	2.51	2.51	39.81
SF-295	0.200	15.85	15.84	10.0	1.58	31.62
SF-539	0.244	19.95	19.95	10.0	1.58	50.12
SNB-19	0.428	19.95	12.58	3.16	3.16	63.09
SNB-75	0.228	15.85	12.58	5.011	3.16	25.12
U251	0.137	15.85	25.12	3.16	1.99	50.12
<i>Melanoma</i>						
LOX IMVI	0.0997	19.95	6.31	3.16	1.58	39.81
MALME-3M	0.44	19.95	1.58	3.98	1.99	39.81
M14	0.171	63.09	6.31	1.995	1.99	31.62
MDA-MB-435	0.623	15.85	19.95	3.16	1.58	31.62
SK-MEL-2	0.307	15.85	6.31	10.0	1.99	39.81
SK-MEL-28	0.340	15.85	50.12	3.16	2.51	39.81
SK-MEL-5	0.223	15.85	19.5	3.16	1.58	25.12
UACC-257	0.340	19.95	100	2.51	1.99	50.12
UACC-62	0.234	15.85	3.16	1.995	1.58	31.62
<i>Ovarian Cancer</i>						
IGROV1	0.196	15.85	0.316	3.16	2.51	100
OVCAR-3	0.125	15.85	3.98	5.011	3.16	50.12
OVCAR-4	0.063	12.58	10.00	6.31	3.16	39.81
OVCAR-5	6.48	19.95	7.94	3.98	3.16	100
OVCAR-8	0.25	19.95	7.94	0.631	3.16	31.62
NCI/ADR-RES	0.324	15.85	7.94	1.26	2.51	31.62
SK-OV-3	0.251	19.95	0.50	1.0	2.51	NT ^b
<i>Renal Cancer</i>						
786-0	0.182	39.81	10.00	3.16	3.16	NT ^b
A498	9.81	15.85	2.51	0.631	2.51	31.62
ACHN	0.117	15.85	0.199	0.158	2.51	39.81
CAKI-1	0.104	19.95	0.199	0.5012	3.16	79.43
RXF 393	0.271	15.85	3.98	3.16	2.51	25.12
SN12C	0.354	15.85	1.58	1.258	2.51	39.81
TK-10	0.207	19.95	0.251	0.794	3.98	63.09
UO-31	0.139	15.85	1.00	1.584	2.51	31.62
<i>Prostate Cancer</i>						
PC-3	0.319	12.58	39.81	5.011	1.99	25.12
DU-145	0.144	15.85	1.99	1.584	3.16	50.12
<i>Breast Cancer</i>						
MCF7	0.253	15.85	100.00	5.011	2.51	31.62
MDA-MB-231/ATCC	0.308	15.85	6.31	3.98	1.26	19.95
HS 578 T	11.7	19.95	6.31	7.94	2.51	79.43
BT-549	0.346	19.95	31.62	3.16	3.16	NT ^b
T-47D	0.39	15.85	3.98	7.94	1.58	31.62
MDA-MB-468	0.203	NT ^b	0.126	0.01258	1.99	19.95

^a<https://dtp.cancer.gov/dtpstandard/dwindex/index.jsp>.^bNT: Not tested.

Table 4. Average antitumor activity of compound **20**, and reference drugs against tumour cell lines from nine different organs at 10-fold dilution of five concentrations; median growth inhibitory (GI_{50} , μM), total growth inhibitory (TGI, μM) and median lethal (LC_{50} , μM)^a.

Compd. No. (NSC) ^c	Activity	Subpanel tumour cell lines									
		leukaemia	NSC lung cancer	colon cancer	CNS cancer	melanoma	ovarian cancer	renal cancer	prostate cancer	breast cancer	MG-MID ^b
20 (799156)	GI_{50}	0.23	0.26	0.27	0.22	0.31	1.10	1.40	0.23	2.20	0.26
	TGI	83.5	65.0	c	71.7	45.6	70.0	80.3	c	69.5	46.8
	LC_{50}	c	c	c	c	c	c	c	c	c	c
Celecoxib (719627)	GI_{50}	12.35	25.09	20.73	17.22	22.46	17.14	19.87	14.22	17.49	17.5
	TGI	29.27	41.93	41.39	31.62	38.49	34.20	41.19	28.37	34.89	34.0
	LC_{50}	67.09	67.08	66.51	58.76	64.31	65.91	61.22	57.01	67/03	63.3
5-Flu (19893)	GI_{50}	2.82	13.59	0.27	14.38	7.83	5.17	0.93	1.46	6.87	0.90
	TGI	68.37	80.45	51.41	73.70	61.57	38.36	46.25	c	68.01	43.4
	LC_{50}	c	c	89.30	c	95.42	92.87	c	c	c	95.6
Erlotinib (718781)	GI_{50}	27.85	13.11	51.68	16.99	23.74	5.52	2.46	20.90	24.72	7.68
	TGI	96.57	73.76	c	82.11	77.89	74.41	42.59	c	70.53	66.3
	LC_{50}	c	97.71	c	c	93.31	97.06	89.15	c	96.43	95.6
Gefitinib (759856)	GI_{50}	2.56	2.05	5.23	5.64	3.68	3.05	1.41	3.29	4.67	2.1
	TGI	12.07	13.86	18.47	19.62	12.49	33.29	12.50	31.62	18.62	14.3
	LC_{50}	93.85	94.68	51.74	50.56	36.40	83.58	52.82	89.72	52.47	51.9
Sorafenib (747971)	GI_{50}	1.91	2.34	2.19	2.33	1.87	2.89	2.86	2.58	2.17	2.33
	TGI	42.12	7.99	7.94	7.64	6.29	14.43	10.86	10.27	9.35	9.11
	LC_{50}	c	49.15	38.06	27.77	28.57	71.34	54.75	69.91	57.29	43.1

^a GI_{50} , molar concentration of the compound that inhibits 50% net cell growth; TGI, molar concentration of the compound leading to total inhibition; and LC_{50} , molar concentration of the compounds leading to 50% net cell death.

^bFull panel mean-graph midpoint (μM).

^c<https://dtp.cancer.gov/dtpstandard/dwindex/index.jsp>.

c: Compounds showed values $\geq 100 \mu\text{M}$.

Bold values used only for more precise comparison.

Table 5. Effect of compounds **6**, **9**, **16**, and **20** and DMSO on the percentage of HL60 cells stained positive for annexin V-FITC

Sample/cell line	Total	Apoptosis		Necrosis
		Early	Late	
6	12.57	3.52	7.64	1.41
9	16.89	5.66	9.04	2.19
16	22.41	7.34	13.41	1.66
20	24.31	8.42	12.66	3.23
DMSO	1.71	0.57	0.22	0.92

alkylphenyl moiety, such as the 4-tolyl fragment in compound **9** and the *N,N*-diethylaminophenyl fragment in compound **20**, have high COX-2 inhibition compared to compounds devoid of the 4-alkylphenyl moiety, such as compounds **6** and **16**.

2.4.2. Kinase inhibition activity

We tested the inhibitory effects of the most active compounds **6**, **9**, **16**, and **20** against EGFR and HER2⁴⁰. We also tested the reference drugs erlotinib, sorafenib, and gefitinib. Table 7 summarises the inhibitory activities of compounds **6**, **9**, **16**, and **20**, and the reference drugs. The IC_{50} of erlotinib, sorafenib, and gefitinib against EGFR was 0.11, 0.10, and 0.055 μM , respectively, and against HER2 was 0.09, 0.05, and 0.079 μM , respectively. The IC_{50} of compounds **6**, **9**, **16**, and **20** against EGFR and HER2 were in the submicromolar range of **0.07–0.77** μM . Compounds **16** and **20** showed the highest and most potent inhibitory activity against EGFR ($IC_{50} = 0.20$ and 0.19, respectively) and HER2 ($IC_{50} = 0.13$ and 0.07 μM , respectively) compared to erlotinib (EGFR- $IC_{50} = 0.11$ and HER2- $IC_{50} = 0.09 \mu\text{M}$), sorafenib (EGFR- $IC_{50} = 0.10$ and HER2- $IC_{50} = 0.05 \mu\text{M}$), and gefitinib (EGFR- $IC_{50} = 0.055$ and HER2- $IC_{50} = 0.079 \mu\text{M}$). Compound **9** was the least active against EGFR and HER2 ($IC_{50} = 0.77$ and 0.41 μM , respectively), while compound **6**

was more effective against EGFR ($IC_{50} = 0.26 \mu\text{M}$) compared to HER2 ($IC_{50} = 0.35 \mu\text{M}$). Compound **20** showed inhibitory activity approximately similar to the reference drugs against EGFR and HER2. Compounds with 2-hydroxyphenyl fragments, such as compounds **16** and **20**, are more potent than corresponding compounds with the 4-tolyl moiety, such as compound **9**, or the 1-naphthyl fragment, such as compound **6**. In the enzymatic assay, the 2-hydroxyphenyl moiety plays a major role in the inhibitory activity against EGFR and HER2.

2.5. Molecular docking study

Molecular modelling is an important tool for studying the biological activity and SARs of bioactive compounds and exploring the binding mode of ligand molecules within the receptor- or putative enzyme-binding sites^{77–80}. We performed molecular docking using the MOE 2008.10 program protocol obtained from Chemical Computing Group Inc. (Montreal, QC, Canada)⁸¹. We subjected the selected compounds and the co-crystallized bound inhibitors to molecular docking into the putative active site of the protein to ensure docking accuracy and generate an appropriate binding orientation^{27,40,41,82,83}.

2.5.1. Molecular docking of compound **9** with COX-2

Molecular docking was performed to study the mode of interaction between the most active compound **9** and the COX-2 pocket-binding site (Figure 6). We derived the crystallographic binding site on the COX-2 isozyme in a complex with the SC-558 ligand, a celecoxib analogue, from the Protein Data Bank (PDB code: 1CX2) (Figure 6, left panel). We used the interaction energy and hydrogen bond formation among compound **9** and the amino acids

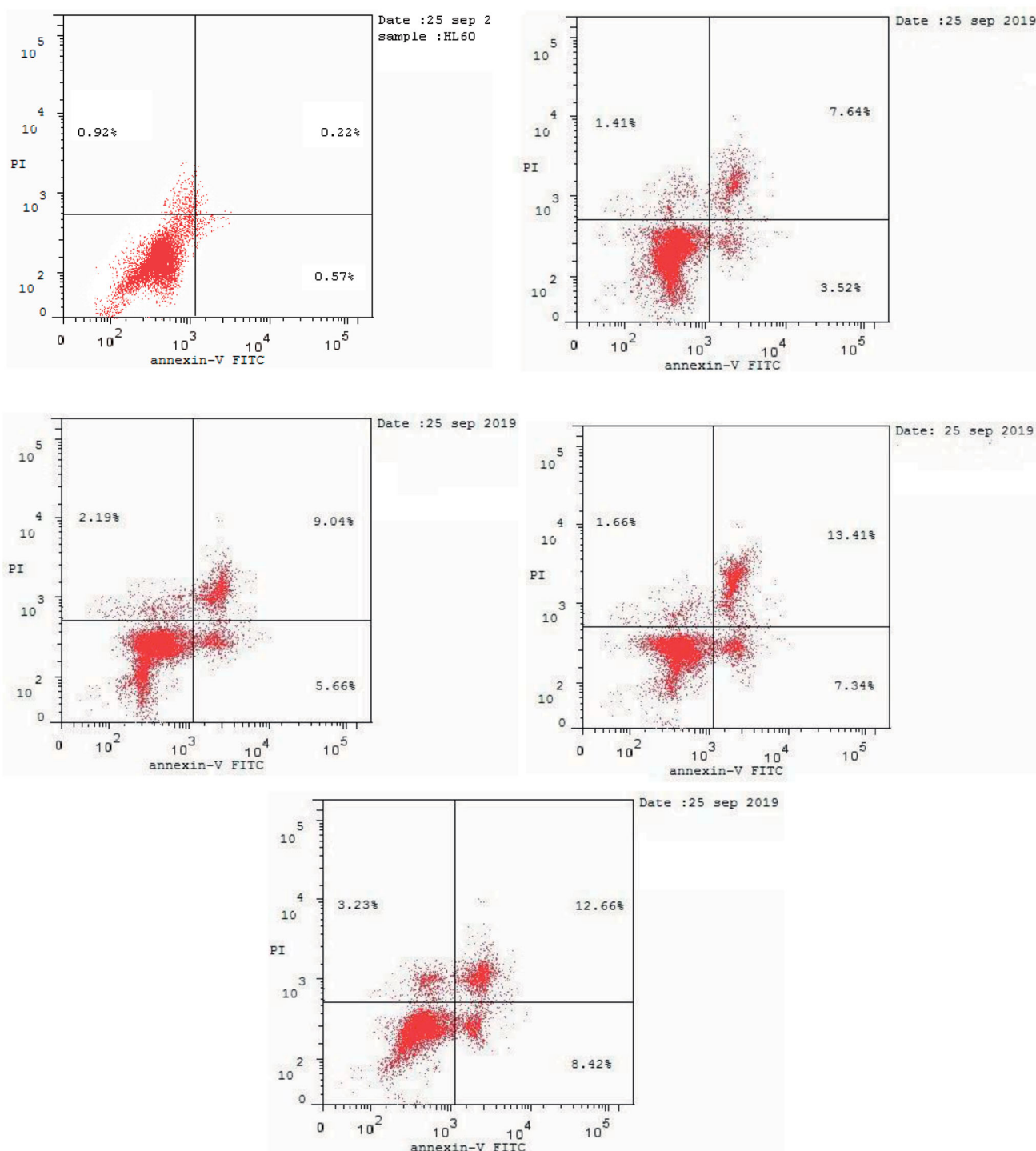


Figure 4. Effect of DMSO (upper left panel), and compounds **6** (upper right panel), **9** (middle left panel), **16** (middle right panel), and **20** (lower panel) on the percentage of annexin V-FITC-positive staining in HL60 cells.

within the putative active pocket of the COX-2 isozyme to predict the mode of interaction. **Figure 6** shows the molecular docking results for compound **9**. Compound **9** was placed into the catalytic site of the COX-2 isozyme, where the pharmacophoric 4-methylsulfonylbenzene group can interact with amino acid residues Ile-517, Phe-518, His-90, Gln-192, and Arg-513 through a network of classical and nonclassical hydrogen bonds. These binding interactions were approximately similar to those of the SC-558 inhibitor co-crystallized in the COX-2-binding site. The stability of the docked complex of the target compound **9** in the COX-2-

binding site depended on the methylsulfonyl pharmacophore ($-\text{SO}_2\text{CH}_3$) by forming classical and nonclassical hydrogen bonds with the key amino acid residues Arg-513 (3.06 Å), Gln-192 (3.26 Å), Ile-517 (3.64 Å), and Phe-518 (3.29 Å) (**Figure 6**, right panel), while the phenyl ring attached to the methylsulfonyl pharmacophore formed two nonclassical hydrogen bonds by binding with amino acid residues His-90 (3.33 Å) and Leu-352 (2.78 Å) and undergoing an additional CH- π interaction with amino acid residue Ser-353 (3.87 Å). Also, the benzylidenehydrazine fragment of compound **9** interacted with amino acid residues

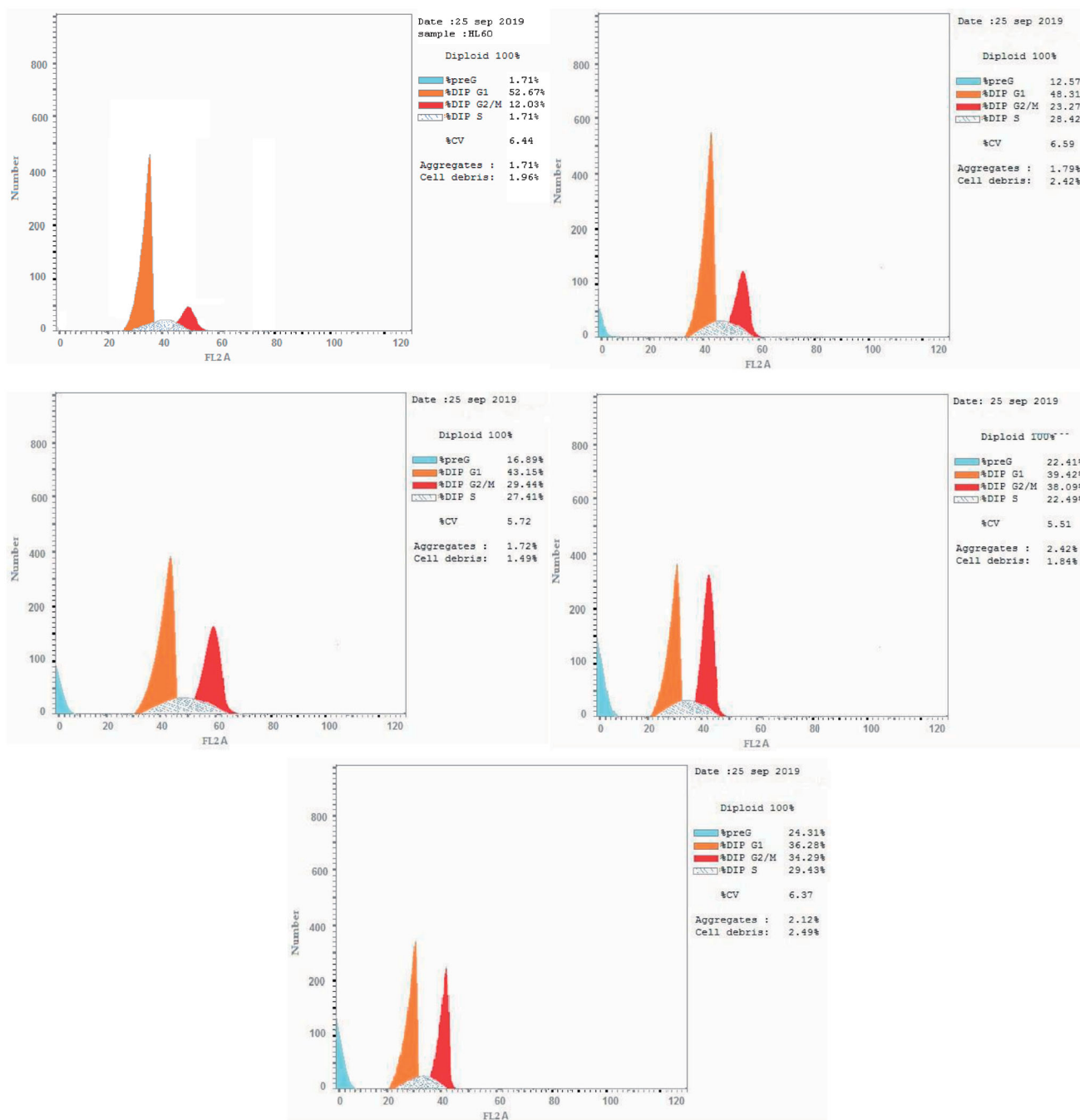


Figure 5. Cell cycle analysis of HL60 cells treated with DMSO (upper left panel) and compounds 6 (upper right panel), 9 (middle left panel), 16 (middle right panel), and 20 (lower panel).

Table 6. Effect of compounds 6, 9, 16, and 20 and DMSO on the cell cycle of HL60 cells.

Sample	Conc. (μM)	%G0-G1	%S	%G2-M	%Pre-G1
6	10.0	48.31	28.42	23.27	12.57
9	10.0	43.15	27.41	29.44	16.89
16	10.0	39.42	22.49	38.09	22.41
20	10.0	36.28	29.43	34.29	24.31
DMSO	0.0	52.67	35.3	12.03	1.71

Ala-527, Val-349, Val-116, Leu-359, and Leu-531 through hydrophobic interactions. The hydrazino fragment of benzylidenehydrazine formed three classical hydrogen bonds with amino acid residues Arg-120 (2.79 Å), Tyr-355 (3.15, and 3.15 Å), while the

Table 7. *In vitro* inhibitory effects of COX-2, EGFR, and HER2 of the antitumor agents 6, 9, 16, and 20.^a

Compound No.	IC ₅₀ (μM) ^a		
	COX-2 Inhibition	EGFR Inhibition	HER2 Inhibition
6	36.27 ± 2.55	0.26 ± 0.09	0.35 ± 0.01
9	2.97 ± 0.07	0.77 ± 0.03	0.41 ± 0.01
16	82.45 ± 3.61	0.20 ± 0.07	0.13 ± 0.04
20	6.94 ± 0.41	0.19 ± 0.01	0.07 ± 0.02
Celecoxib	2.79 ± 0.07	–	–
Erlotinib	–	0.11 ± 0.04	0.09 ± 0.03
Sorafenib	–	0.10 ± 0.04	0.05 ± 0.02
Gefitinib	–	0.055 ± 0.99	0.079 ± 1.42

^aIC₅₀ value is the compound concentration required to produce 50% inhibition.

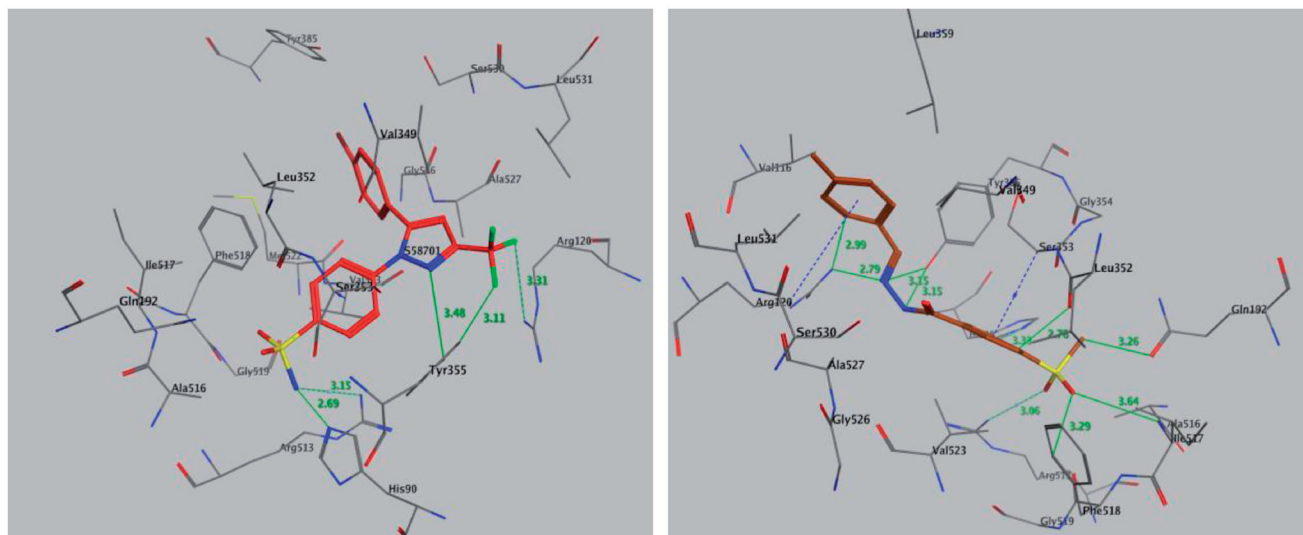


Figure 6. Binding mode of co-crystallized inhibitor (upper panel), compounds **9** (middle panel), and **20** (lower panel) within COX-2 binding site (PDB ID: 1CX2).

phenyl part of the benzylidenehydrazine moiety interacted with the amino acid residue Arg-120 by forming a nonclassical H-bond (2.99 Å) and CH- π interaction (3.98 Å) (Figure 6, right panel).

2.5.2. Molecular docking of compound **20** with EGFR

The results of the antitumor activity and enzymatic assay of compound **20** against EGFR prompted us to perform molecular docking studies of the ATP-binding site of EGFR, along with the reference drug erlotinib to predict the binding interactions of the target compound (Figure 7). We retrieved the ligand erlotinib from the PDB as a co-crystallized ligand in a complex with EGFR (PDB code: 1M17) (Figure 7, left panel). Both phenyl rings of compound **20** surrounded and interacted with amino acid residues lining the hydrophobic pocket in EGFR-TK, such as Gly-772, Leu-768, Pro-770, Leu-694, Leu-820, and Val-702 (Figure 7, right panel). Also, the -OH group of compound **20** formed triple hydrogen bonds with amino acid residues Met-769 (3.19 Å), Pro-770 (3.49 Å), and Gly-772 (3.73 Å). The methylsulfonyl ($\text{CH}_3\text{-SO}_2\text{-}$) moiety showed significant interactions, where the oxygen atom of the $\text{CH}_3\text{-SO}_2\text{-}$ group directly formed hydrogen bonds with the amino acid residue Thr-766 (3.26 Å) and the Thr-830 side chain (3.00 Å) and showed additional binding with a water molecule (HOH-10)-mediated hydrogen bonding with Thr-766 (2.78, and 3.10 Å). Also, the methyl moiety of the $\text{CH}_3\text{-SO}_2\text{-}$ group interacted with amino acid residue Met-742 by a nonclassical hydrogen bond of 3.91 Å with the sulphur (S-) part of Met-742, while the phenyl part attached to the methylsulfonyl moiety interacted with amino acid residue Leu-820 through CH- π interaction (4.34 Å). These binding interactions indicated that both 2-hydroxyphenyl and 4-methylsulfonylbenzene fragments are important for binding and subsequent inhibitory effects (Figure 7).

2.5.3. Molecular docking of compound **20** with HER2

We retrieved the crystal 3D structure of HER2 co-crystallized with its bound inhibitor O3Q from the PDB (PDB code: 3PP0) (Figure 8, left panel). Molecular docking of compound **20** into the HER2-binding cavity showed that the 2-hydroxyphenyl fragment forms four hydrogen bonds with amino acid residues Leu-796 (2.95 Å), Thr-798 (3.81 Å), Ala-751 (3.65 Å), and Lys-753 (3.61 Å), while the

hydrazide fragment forms two hydrogen bonds with a water molecule (HOH-22)-mediated hydrogen bonding with Thr-862 (2.45, and 3.05 Å) (Figure 8, right panel). In addition, we observed one more hydrogen bond between one oxygen of the sulphonyl group and the amino acid residue Cys-805 (2.50 Å). In contrast, the *N,N*-diethylaminophenyl moiety of compound **20** shows hydrophobic interactions with the side chains of amino acid residues Glu-770, Ser-783, Leu-785, Met-774, Phe-864, Leu-796, Thr-798, Asp-863, and Lys-753, while the methylsulfonylbenzene moiety showed hydrophobic interactions with amino acid residues Leu-852, Met-801, Leu-800, Val-734, Leu-826, and Gly-804. The binding modes of compound **20** are approximately similar to the co-crystallized bound inhibitor with HER2 kinase.

2.6. Physicochemical and pharmacokinetic predictions

We predicted the pharmacokinetic and physicochemical properties of the most active compounds **6**, **9**, **16**, **20**, and reference drugs celecoxib, erlotinib, gefitinib, and vismodegib using the automated SwissADME online calculation system (Table 8)⁸⁴. Compounds **6**, **9**, **16**, **20** showed high gastrointestinal absorption, while compound **20** was predicted as an inhibitor of CYP2C19, CYP2C9, and CYP3A4 isoforms and a non-inhibitor of CYP1A2 and CYP2D6 isoforms (Table 8). In contrast, compound **16** was predicted as a non-inhibitor of all CYP isoforms. In addition, compounds **6** and **9** were predicted as inhibitors of CYP2C19 and CYP1A2 isoforms and non-inhibitors of CYP2C9, CYP3A4, and CYP2D6 isoforms. In addition, we calculated the drug-likeness properties, as indicated by major Lipinski's (Pfizer), Ghose's (Amgen), Veber's (GSK), and Egan's (Pharmacia) pharmaceutical rules^{85–87}. Compounds **6**, **9**, **16**, **20** successfully passed all filters (Table 8). The BOILED-Egg graph⁸⁸ of the WlogP/tPSA (topological polar surface area) showed that compounds **6**, **9**, **16**, **20**, together with celecoxib and vismodegib, are located in the human intestinal absorption (HIA) region with no BBB permeation, indicating few CNS side effects (Figure 9). Indeed, compounds **6**, **9**, **16**, **20** are not P-glycoprotein (P-gp-) substrates, suggesting that they are not susceptible to the efflux mechanism carried out by P-gp that is used by many cancer cell lines as a drug resistance mechanism (Figure 9)^{89–91}. In addition, the bioavailability radar chart of compounds **6**, **9**, **16**, **20**, and reference drugs are shown in

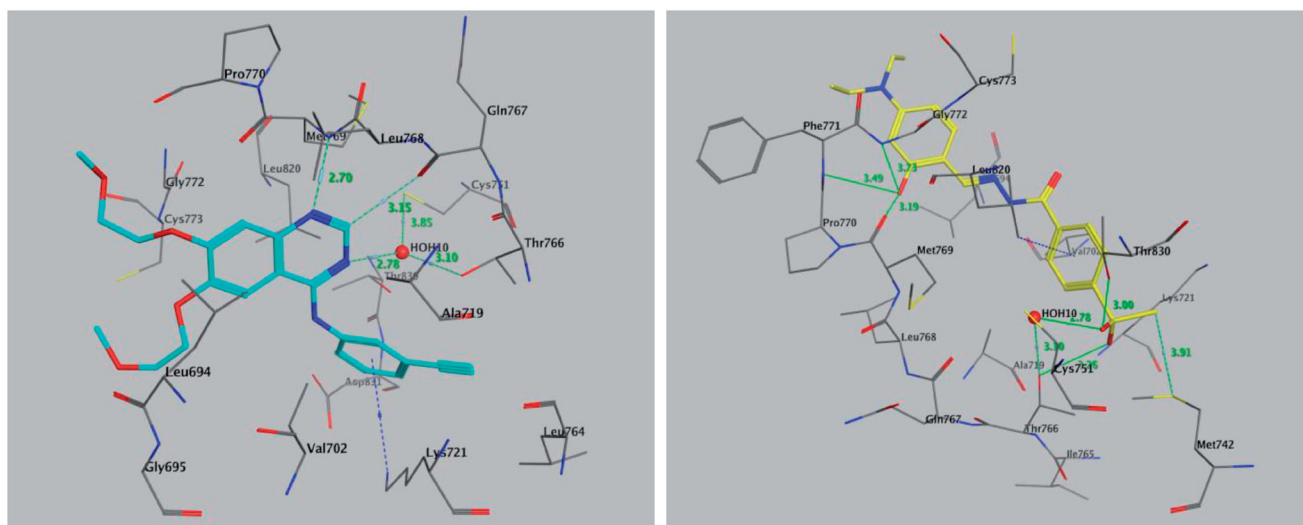


Figure 7. Binding mode of co-crystallized inhibitor (left panel) and compounds **20** (right panel) within EGFR binding site (PDB ID: 1M17).

Figures 10 and 11. These charts were drawn as six axes for six key properties of oral bioavailability: polarity (POLAR), solubility (INSOLU), lipophilicity (LIPO), flexibility (FLEX), saturation (INSATU), and size (SIZE)^{89–91}. The optimal property ranges are shown as a pink area, while the red line represents predicted properties for the examined molecule. The SwissADME tool calculation of compounds **6**, **9**, **16**, and **20** predicts that they possess appropriate physicochemical and pharmacokinetic properties.

3. Conclusion

We synthesised a series of hydrazones **4–24** based on a 4-methylsulfonylbenzene scaffold starting from 4-methylsulfonylphenylhydrazide. We also analysed the potential antitumor activities of the 21 hydrazones using 59 human cell lines and performed enzyme inhibition assays using EGFR, HER2, and COX-2. Compounds **6**, **9**, **16**, and **20** possess the highest broad-spectrum and potent antitumor activity with a GI of >10–100% and a PCE of 52/59, 27/59, 59/59, and 59/59, respectively, for nine human tissue compared to imatinib (GI = >10%–47.1%; PCE = 20/55). The antitumor activity of compounds **6**, **9**, **16**, and **20** against individual organs is GI = 20.8–100% for leukaemia, 12.7%–96.7% for NSCLC, 13.9%–91.4% for colon cancer, 10.3%–96.0% for CNS cancer, 10.6–100% for melanoma, 12.3%–83.2% for ovarian cancer, 12.3–100% for renal cancer, 11.2%–75.5% for prostate cancer, and 12.4%–98.8% for breast cancer. Compound **20** has the highest GI and shows significant antitumor activity ($GI_{50} = 0.063$ – $11.7 \mu\text{M}$) compared to celecoxib, erlotinib, gefitinib, sorafenib, and vismodegib ($GI_{50} = 3.98$ – 63.09 , 0.10 – 100.0 , 0.0125 – 10.0 , 1.26 – 3.98 , and 19.95 – $100.0 \mu\text{M}$, respectively). Cell cycle analysis showed that the apoptotic mechanism underlying programmed cell death is the main mechanism rather than the necrotic pathway, and compounds **6**, **9**, **16**, and **20** induce apoptosis by inhibiting cell growth at the G2/M phase. In addition, compounds **9** and **20** are the most active inhibitory agents against COX-2 ($IC_{50} = 2.97$ and $6.94 \mu\text{M}$, respectively) compared celecoxib ($IC_{50} = 2.79 \mu\text{M}$), while compounds **16** and **20** have the highest inhibition activity against EGFR ($IC_{50} = 0.2$ and $0.19 \mu\text{M}$, respectively) and HER2 ($IC_{50} = 0.13$ and $0.07 \mu\text{M}$, respectively) compared to erlotinib (EGFR- $IC_{50} = 0.11$ and HER2- $IC_{50} = 0.09 \mu\text{M}$), sorafenib (EGFR- $IC_{50} = 0.10$ and HER2- $IC_{50} = 0.05 \mu\text{M}$), and gefitinib (EGFR- $IC_{50} = 0.055$ and HER2- $IC_{50} = 0.079 \mu\text{M}$). The results as mentioned above indicated that these compounds are

potential multitarget agents as COX-2, EGFR, and HER2 inhibitors. Compound **9** was subjected to molecular docking into binding sites of COX-2, while compound **20** was subjected to molecular docking into the putative binding sites of EGFR and HER2 to find the binding mode and molecular models required for interaction of these compounds with respective enzymes or receptors. Molecular docking showed that the respective molecules bound approximately similar to the co-crystallized inhibitors in COX-2-, EGFR-, and HER2-binding sites. SwissADME and drug-likeness prediction showed that compounds **6**, **9**, **16**, and **20** possess good physicochemical, pharmacokinetic, and drug-likeness properties.

4. Experimental

4.1. Chemistry

Melting points (uncorrected) were recorded on a Barnstead 9100 Electrothermal melting apparatus (APS Water Services Corporation, Van Nuys, CA, USA), while the IR spectra were recorded on a FT-IR Perkin-Elmer spectrometer (PerkinElmer Inc., Waltham, MA, USA). The ^1H NMR and ^{13}C NMR were measured in DMSO- d_6 or CDCl_3 , on Bruker 700 or 500 and 176 or 125 MHz instruments, respectively (Bruker, Billerica, MA, USA). Chemical shifts are reported in δ ppm. Mass spectra were recorded on an Agilent 6320 Ion Trap mass spectrometer (Agilent Technologies, Santa Clara, CA, USA). C, H, and N were analysed at the Research Centre, College of Pharmacy, King Saud University, Saudi Arabia. The results were within $\pm 0.4\%$ of the theoretical values. Compounds **3**, **11**, **16**, **19**, and **20** were prepared according to a previous report⁶⁵.

4.1.1. General procedure for the synthesis of hydrazones 4–24 (Scheme 1)

A mixture of 4-(methylsulfonyl)benzohydrazide **3** (10 mmol) and an appropriate aromatic aldehyde (10 mmol) was stirred in methanol (10 ml) containing a catalytic amount of acetic acid (0.5 ml) at room temperature for 24 h. The obtained solid was filtered, dried, and recrystallized from absolute ethanol.

4.1.1.1. N'-Benzylidene-4-(methylsulfonyl)benzohydrazide (4). M.p 273–275 $^\circ$; 95% yield; IR (KBr, cm^{-1}): 3215 (NH), 1656 (C=O), 1284, 1148 (O=S=O); ^1H NMR (700 MHz, DMSO- d_6): δ 12.10 (s, 1H), 8.48 (s, 1H), 8.16 (d, 2H, $J = 7.77$ Hz), 8.11 (d, 2H, $J = 7.77$ Hz),

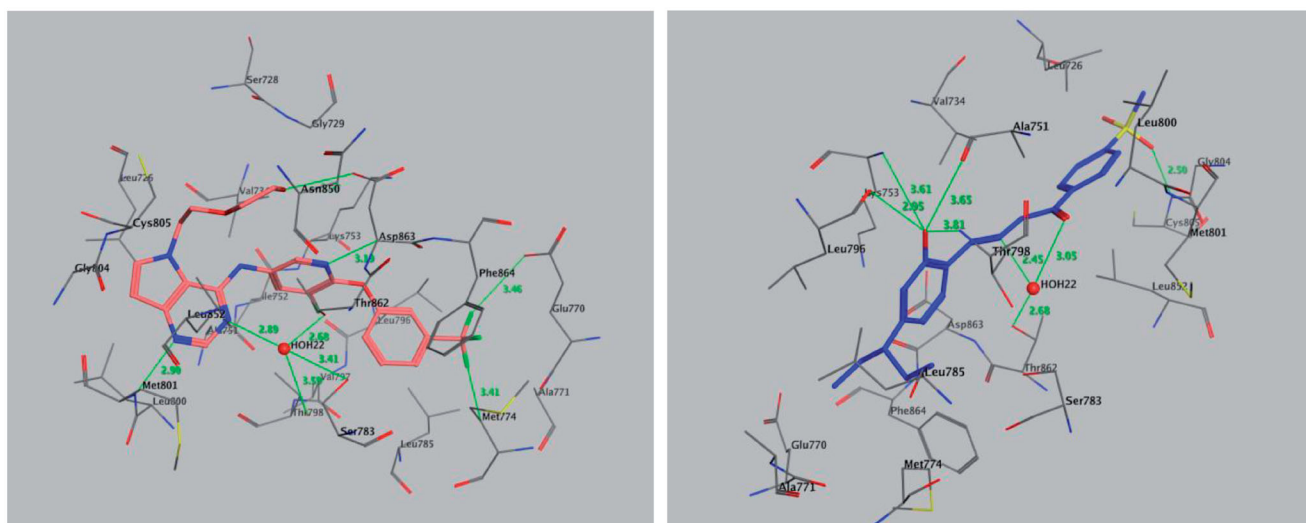


Figure 8. Binding mode of co-crystallized inhibitor (left panel) and compounds 20 (right panel) within HER2 binding site (PDB ID: 3PP0).

Table 8. Predictions of the physicochemical and pharmacokinetic properties for target compounds 6, 9, 16, and 20 together with reference drugs^a

Compounds No.	6	9	16	20	celecoxib	Erlotinib	Gefitinib	Vismodegib
BBB ^b	NO	NO	NO	NO	NO	Yes	Yes	NO
GIA ^b	High	High	High	High	High	High	High	High
P-gp ^b substrate	No	No	No	No	No	No	No	No
CYP1A2 inhibitor ^b	Yes	Yes	No	No	No	Yes	No	No
CYP2C19 inhibitor ^b	Yes	Yes	No	Yes	No	Yes	Yes	Yes
CYP2C9 inhibitor ^b	No	No	No	Yes	Yes	Yes	Yes	Yes
CYP2D6 inhibitor ^b	No	No	No	No	No	Yes	Yes	No
CYP3A4 inhibitor ^b	No	No	No	Yes	No	Yes	Yes	Yes
Log S (Water Solubility)	-6.96 (Poorly soluble)	-5.69 (Moderately soluble)	-4.73 (Moderately soluble)	-5.60 (Moderately soluble)	-6.22 (Poorly soluble)	-7.26 (Poorly soluble)	-7.94 (Poorly soluble)	-8.51 (Poorly soluble)
Bioavailability Score	0.55	0.55	0.55	0.55	0.55	0.55	0.55	0.55
Lipinski #violations	0	0	0	0	0	0	0	0
Ghose #violations	0	0	0	0	1	0	0	1
Veber #violations	0	0	0	0	0	0	0	0
Egan #violations	0	0	0	0	0	0	0	0

^aAll calculations were performed using SwissADME.

^bGIA: gastrointestinal absorption; BBB: blood-brain barrier permeation; P-gp: permeability glycoprotein; CYP1A2, CYP2C9, CYP2C19, CYP3A4 and CYP2D6 are isoforms of cytochromes P450.

7.77 (d, 2H, $J = 7.14$ Hz), 7.48 (dd, 3H, $J = 19.95$ & 7.14 Hz), 3.31 (s, 3H); ¹³C NMR (176 MHz, DMSO-*d*₆): δ 162.3, 149.2, 143.7, 138.3, 134.5, 130.8, 129.3, 129.1, 127.7, 127.6, 43.7; C₁₅H₁₄N₂O₃S: m/z (302.1).

4.1.1.2. 4-(Methylsulfonyl)-N'-(pyridin-3-ylmethylene)benzohydrazide (5). M.p 339–341°; 89% yield; IR (KBr, cm⁻¹) ν : 3221 (NH), 1640 (C=O), 1339, 1147 (O=S=O); ¹H NMR (700 MHz, DMSO-*d*₆): δ 12.26 (s, 1H), 8.89 (s, 1H), 8.64 (d, 1H, $J = 4.55$ Hz), 8.53 (s, 1H), 8.16 (d, 3H, $J = 10.57$, 8.33 Hz), 8.11 (d, 2H, $J = 8.12$ Hz), 7.51 (dd, 1H, $J = 12.53$, 2.80 Hz), 3.31 (s, 3H); ¹³C NMR (176 MHz, DMSO-*d*₆): δ 162.4, 151.4, 149.3, 146.4, 143.8, 138.1, 134.0, 130.4, 129.1, 127.6, 124.5, 43.7; C₁₄H₁₃N₃O₃S: m/z (303.3).

4.1.1.3. 4-(Methylsulfonyl)-N'-(naphthalen-1-ylmethylene)benzohydrazide (6). M.p 235–237°; 88% yield; IR (KBr, cm⁻¹) ν : 3222 (NH), 1651 (C=O), 1295, 1144 (O=S=O); ¹H NMR (700 MHz, DMSO-*d*₆): δ 12.18 (s, 1H), 9.12 (s, 1H), 8.05 (dd, 1H, $J = 15.47$ & 8.19 Hz), 8.21 (d, 2H, $J = 7.63$ Hz), 8.14 (d, 2H, $J = 7.63$ Hz), 8.05 (dd, 2H, $J = 15.47$ & 8.19 Hz), 7.97 (d, 1H, $J = 7.07$ Hz), 7.70 (t, 1H, $J = 15.12$ Hz), 7.63

(dd, 2H, $J = 7.09$ Hz), 3.32 (s, 3H); ¹³C NMR (176 MHz, DMSO-*d*₆): δ 162.3, 149.1, 143.8, 138.3, 134.0, 131.3, 130.6, 129.7, 129.3, 129.1, 128.6, 127.9, 127.7, 126.8, 126.0, 124.7, 43.7; C₁₉H₁₆N₂O₃S: m/z (352.1).

4.1.1.4. N'-(4-Chlorobenzylidene)-4-(methylsulfonyl)benzohydrazide (7). M.p 268–270°; 92% yield; IR (KBr, cm⁻¹) ν : 3239 (NH), 1656 (C=O), 1284, 1145 (O=S=O); ¹H NMR (700 MHz, DMSO-*d*₆): δ 12.16 (s, 1H), 8.46 (s, 1H), 8.16 (d, 2H, $J = 8.26$ Hz), 8.11 (d, 2H, $J = 8.33$ Hz), 7.78 (d, 2H, $J = 8.40$ Hz), 7.54 (d, 2H, $J = 8.33$ Hz), 3.30 (s, 3H); ¹³C NMR (176 MHz, DMSO-*d*₆): δ 162.4, 147.8, 143.8, 138.2, 135.2, 133.4, 129.4, 129.3, 129.1, 127.6, 43.7; C₁₅H₁₃ClN₂O₃S: m/z: 336.0, (M + 2); 338.0.

4.1.1.5. N'-(4-Fluorobenzylidene)-4-(methylsulfonyl)benzohydrazide (8). M.p 278–280°; 90% yield; IR (KBr, cm⁻¹) ν : 3239 (NH), 1655 (C=O), 1285, 1146 (O=S=O); ¹H NMR (700 MHz, DMSO-*d*₆): δ 12.17 (s, 1H), 8.48 (s, 1H), 8.16 (d, 2H, $J = 7.98$ Hz), 8.11 (d, 2H, $J = 5.39$ Hz), 7.82 (t, 2H, $J = 13.09$ Hz), 7.32 (t, 2H, $J = 8.43$ Hz), 3.31 (s, 3H); ¹³C NMR (176 MHz, DMSO-*d*₆): δ 164.4, 163.0, 162.3, 148.0,

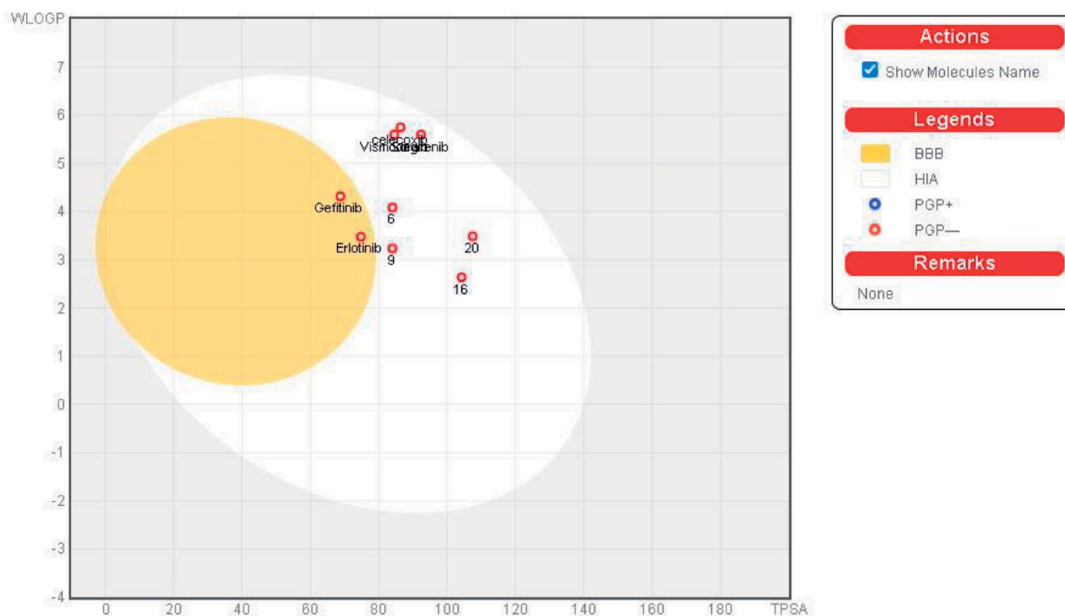


Figure 9. Boiled-Egg plot predicted by swissADME online web tool for target molecules **6**, **9**, **16**, **20**, and the reference drugs (celecoxib, erlotinib, gefitinib, and vismodegib).

143.7, 138.3, 131.2, 131.1, 130.7, 129.9, 129.8, 129.1, 127.6, 116.5, 116.3, 43.7; C₁₅H₁₃FN₂O₃S; m/z: 320.2.

4.1.1.6. N'-(4-Methylbenzylidene)-4-(methylsulfonyl)benzohydrazide (9). M.p 271–272°; 94% yield; IR (KBr, cm⁻¹) ν : 3199 (NH), 1652 (C=O), 1292, 1150 (O=S=O); ¹H NMR (700 MHz, DMSO-d₆): δ 12.04 (s, 1H), 8.44 (s, 1H), 8.16 (d, 2H, *J* = 8.12 Hz), 8.11 (d, 2H, *J* = 8.19 Hz), 7.65 (d, 2H, *J* = 7.84 Hz), 7.29 (d, 2H, *J* = 7.84 Hz), 3.30 (s, 3H), 2.35 (s, 3H); ¹³C NMR (176 MHz, DMSO-d₆): δ 162.3, 149.2, 143.7, 140.7, 138.4, 131.8, 129.9, 129.1, 127.7, 127.6, 43.7, 21.5; C₁₆H₁₆N₂O₃S m/z: 316.4.

4.1.1.7. N'-(4-Methoxybenzylidene)-4-(methylsulfonyl)benzohydrazide (10). M.p 249–251°; 88% yield; IR (KBr, cm⁻¹) ν : 3212 (NH), 1698 (C=O), 1282, 1149 (O=S=O); ¹H NMR (700 MHz, DMSO-d₆): δ 12.08 (s, 0.25H), 11.97 (s, 0.75H), 8.84 (s, 0.25H), 8.42 (s, 0.75H), 8.18 (d, 0.58H, *J* = 8.12 Hz), 8.15 (d, 1.42H, *J* = 8.12 Hz), 8.10 (d, 1.77H, *J* = 8.12 Hz), 8.01 (d, 0.23H, *J* = 7.91 Hz), 7.90 (d, 0.3H, *J* = 7.56 Hz), 7.71 (d, 1.7H, *J* = 8.12 Hz), 7.13 (d, 0.3H, *J* = 8.33 Hz), 7.04 (d, 1.7H, *J* = 8.33 Hz), 3.88 (s, 0.8H), 3.82 (s, 2.2H), 3.30 (s, 3H); ¹³C NMR (176 MHz, DMSO-d₆): δ 162.1, 161.4, 158.3, 149.0, 144.9, 144.6, 143.7, 143.6, 138.5, 138.3, 129.3, 129.1, 129.0, 127.6, 127.0, 114.8, 56.1, 55.7, 43.75; C₁₆H₁₆N₂O₄S m/z: 332.3.

4.1.1.8. N'-(4-(Dimethylamino)benzylidene)-4-(methylsulfonyl)benzohydrazide (12). M.p 295–297°; 85% yield; IR (KBr, cm⁻¹) ν : 3488 (NH), 1655 (C=O), 1278, 1148 (O=S=O); ¹H NMR (700 MHz, DMSO-d₆): δ 11.81 (s, 1H), 8.34 (s, 1H), 8.14 (d, 2H, *J* = 7.77 Hz), 8.09 (d, 2H, *J* = 7.91 Hz), 7.57 (d, 2H, *J* = 8.12 Hz), 7.63 (d, 2H, *J* = 8.19 Hz), 3.30 (s, 3H), 2.97 (s, 5.3H), 2.92 (s, 0.7H); ¹³C NMR (176 MHz, DMSO-d₆): δ 161.8, 152.1, 150.0, 143.5, 138.7, 130.7, 129.1, 129.0, 127.6, 121.7, 112.2, 49.0, 43.7; C₁₇H₁₉N₃O₃S m/z: 345.1.

4.1.1.9. N'-(2-Chlorobenzylidene)-4-(methylsulfonyl)benzohydrazide (13). M.p 346–348°; 85% yield; IR (KBr, cm⁻¹) ν : 3278 (NH), 1684 (C=O), 1271, 1142 (O=S=O); ¹H NMR (700 MHz, DMSO-d₆): δ

12.31 (s, 1H), 8.89 (s, 1H), 8.19 (s, 1H), 8.18 (d, 2H, *J* = 8.12 Hz), 8.11 (d, 2H, *J* = 8.19 Hz), 8.05 (d, 2H, *J* = 7.14 Hz), 7.55 (d, 1H, *J* = 7.56 Hz), 7.47 (p, 2H, *J* = 16.31, 7.14 & 7.0 Hz), 3.31 (s, 3H); ¹³C NMR (176 MHz, DMSO-d₆): δ 162.4, 145.0, 143.9, 138.0, 133.8, 132.2, 131.8, 130.4, 129.2, 128.1, 127.6, 127.4, 43.7; m/z: C₁₅H₁₃CIN₂O₃S m/z 336.0, (M + 2; 338.0).

4.1.1.10. N'-(2-Fluorobenzylidene)-4-(methylsulfonyl)benzohydrazide (14). M.p 300–302°; 88% yield; IR (KBr, cm⁻¹) ν : 3211 (NH), 1654 (C=O), 1280, 1144 (O=S=O); ¹H NMR (700 MHz, DMSO-d₆): δ 12.21 (s, 1H), 8.72 (s, 1H), 8.18 (d, 2H, *J* = 8.12 Hz), 8.11 (d, 2H, *J* = 8.12 Hz), 7.98 (t, 1H, *J* = 7.31 Hz), 7.52 (dd, 1H, *J* = 6.72, 6.93 Hz), 7.33 (d, 2H, *J* = 7.98 Hz), 3.31 (s, 3H); ¹³C NMR (176 MHz, DMSO-d₆): δ 162.3, 162.0, 160.6, 143.9, 141.9, 141.8, 138.1, 132.8, 132.7, 129.1, 127.7, 126.8, 125.4, 122.1, 122.0, 116.5, 43.7; C₁₅H₁₃FN₂O₃S m/z: 320.2.

4.1.1.11. N'-(2-Methoxybenzylidene)-4-(methylsulfonyl)benzohydrazide (15). M.p 333–335°; 91% yield; IR (KBr, cm⁻¹) ν : 3198 (NH), 1679 (C=O), 1276, 1145 (O=S=O); ¹H NMR (700 MHz, DMSO-d₆): δ 12.08 (s, 1H), 8.84 (s, 1H), 8.18 (d, 2H, *J* = 7.56 Hz), 8.09 (d, 2H, *J* = 7.63 Hz), 7.90 (d, 1H, *J* = 7.70 Hz), 7.44 (t, 1H, *J* = 7.73 Hz), 7.13 (d, 1H, *J* = 8.33 Hz), 7.04 (t, 1H, *J* = 7.42 Hz), 3.82 (s, 3H), 3.31 (s, 3H); ¹³C NMR (176 MHz, DMSO-d₆): δ 162.1, 158.3, 144.6, 143.7, 138.3, 132.3, 129.1, 127.6, 126.0, 122.5, 121.2, 112.3, 56.1, 43.7; C₁₆H₁₆N₂O₄S m/z: 332.1.

4.1.1.12. N'-(2,4-Dichlorobenzylidene)-4-(methylsulfonyl)benzohydrazide (17). M.p > 350°; 93% yield; IR (KBr, cm⁻¹) ν : 3227 (NH), 1677 (C=O), 1294, 1150 (O=S=O); ¹H NMR (700 MHz, DMSO-d₆): δ 12.35 (s, 1H), 8.83 (s, 1H), 8.18 (d, 2H, *J* = 7.84 Hz), 8.11 (d, 2H, *J* = 7.77 Hz), 8.05 (d, 1H, *J* = 8.47 Hz), 7.75 (s, 1H), 7.55 (d, 1H, *J* = 8.47 Hz), 3.31 (s, 3H); ¹³C NMR (176 MHz, DMSO-d₆): δ 162.4, 143.9, 137.9, 135.8, 134.5, 130.9, 129.9, 129.2, 128.6, 127.7, 43.7; C₁₅H₁₂Cl₂N₂O₃S; m/z 371.0, (M + 2; 373).

4.1.1.13. N'-(3,4-Dichlorobenzylidene)-4-(methylsulfonyl)benzohydrazide (18). M.p 242–244°; 87% yield; IR (KBr, cm⁻¹) ν : 3282 (NH),

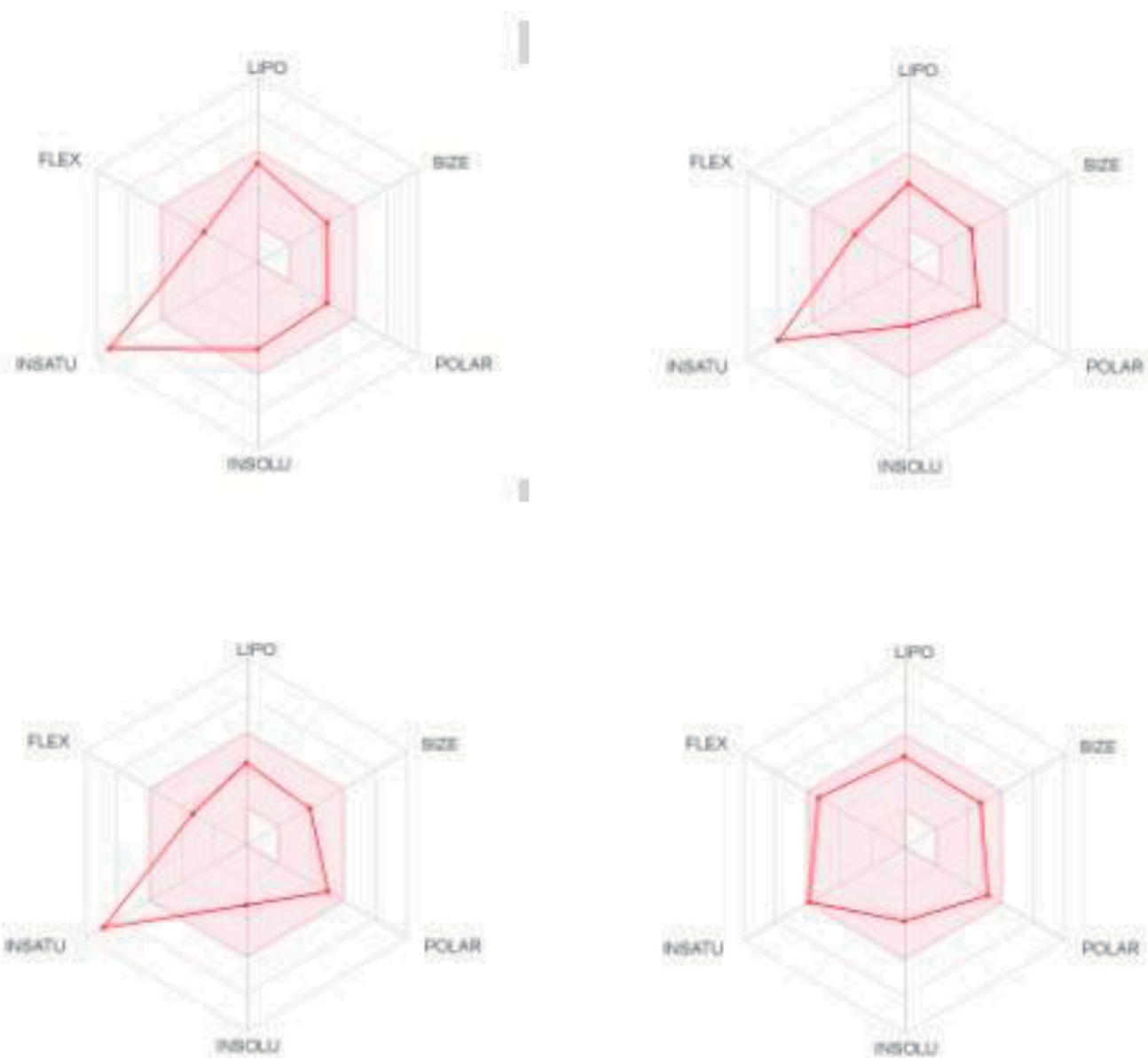


Figure 10. Bioavailability radar charts as predicted by swissADME online web tool for target molecules **6** (upper left panel), **9** (upper right panel), **16** (lower left panel), and **20** (lower right panel).

1688 (C=O), 1274, 1146 (O=S=O); ^1H NMR (700 MHz, DMSO- d_6): δ 12.29 (s, 1H), 8.44 (s, 1H), 8.15 (d, 2H, $J=8.05$ Hz), 8.11 (d, 2H, $J=8.05$ Hz), 7.99 (s, 1H), 7.76 (dd, 2H, $J=8.12$ & 7.84 Hz), 3.30 (s, 3H); ^{13}C NMR (176 MHz, DMSO- d_6): δ 162.5, 146.4, 143.9, 138.0, 135.4, 132.9, 132.2, 131.6, 129.2, 129.1, 127.6, 127.4, 43.7; C₁₅H₁₂Cl₂N₂O₃S: m/z 371.0, (M + 2; 373).

4.1.1.14. *N'*-(3,4-Dimethoxybenzylidene)-4-(methylsulfonyl)benzohydrazide (21). M.p 245–247°; 90% yield; IR (KBr, cm^{-1}) ν : 3212 (NH), 1657 (C=O), 1269, 1140 (O=S=O); ^1H NMR (700 MHz, DMSO- d_6): δ 11.97 (s, 1H), 8.39 (s, 1H), 8.14 (d, 2H, $J=8.19$ Hz), 8.09 (d, 2H, $J=8.19$ Hz), 7.37 (s, 1H), 7.24 (d, 1H, $J=8.05$ Hz), 7.05 (d, 1H, $J=8.26$ Hz), 3.83 (s, 3H), 3.82 (s, 3H), 3.30 (s, 3H); ^{13}C NMR (176 MHz, DMSO- d_6): δ 172.5, 162.2, 151.4, 149.5, 149.3, 143.6, 138.5, 129.0, 127.6, 122.6, 111.9, 108.6, 56.0, 55.9, 43.7; C₁₇H₁₈N₂O₅S m/z: 362.3.

4.1.1.15. *N'*-(Benzo[d][1,3]dioxol-5-ylmethylene)-4-(methylsulfonyl)benzohydrazide (22). M.p 289–291°; 86% yield; IR (KBr, cm^{-1}) ν : 3220 (NH), 1655 (C=O), 1275, 1145 (O=S=O); ^1H NMR (700 MHz, DMSO- d_6): δ 12.00 (s, 1H), 8.38 (s, 1H), 8.14 (d, 2H, $J=8.19$ Hz), 8.09 (d, 2H, $J=8.19$ Hz), 7.33 (s, 1H), 7.20 (d, 1H, $J=7.91$ Hz), 7.02 (d, 1H, $J=7.91$ Hz), 6.11 (s, 2H), 3.30 (s, 3H); ^{13}C NMR (176 MHz, DMSO- d_6): δ 162.2, 149.7, 148.9, 148.5, 143.7, 138.4, 129.0, 128.9, 127.6, 124.1, 108.9, 105.6, 102.1, 43.7; C₁₆H₁₄N₂O₅S m/z: 346.2.

4.1.1.16. 4-(Methylsulfonyl)-*N'*-(3,4,5-trimethoxybenzylidene)benzohydrazide (23). M.p 228–230°; 95% yield; IR (KBr, cm^{-1}) ν : 3199 (NH), 1668 (C=O), 1272, 1132 (O=S=O); ^1H NMR (700 MHz, DMSO- d_6): δ 12.09 (s, 1H), 8.40 (s, 1H), 8.14 (d, 2H, $J=8.19$ Hz), 8.09 (d, 2H, $J=8.05$ Hz), 7.06 (s, 2H), 3.85 (s, 6H), 3.72 (s, 3H), 3.30 (s, 3H); ^{13}C NMR (176 MHz, DMSO- d_6): δ 162.4, 153.6, 149.1, 143.7,

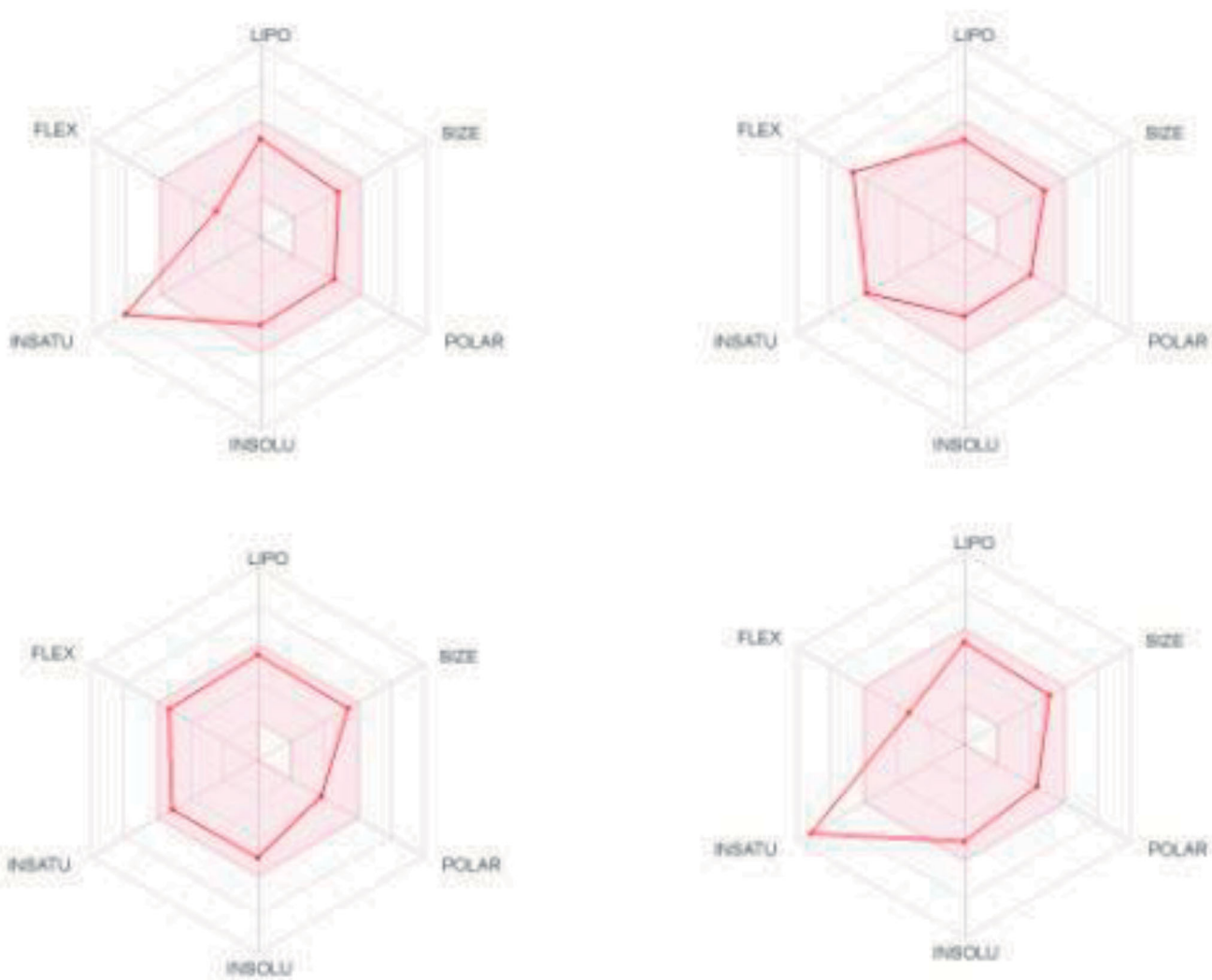


Figure 11. Bioavailability radar charts as predicted by swissADME online web tool for reference drugs celecoxib (upper left panel), erlotinib (upper right panel), gefitinib (lower left panel), and vismodegib (lower right panel).

139.8, 138.4, 130.0, 129.1, 127.6, 1104.8, 60.6, 56.4, 43.7; C₁₈H₂₀N₂O₆S m/z: 392.1.

4.1.1.17. (4-(Methylsulfonyl)-N'-(2,4,5-trimethoxybenzylidene)benzohydrazide (24). M.p 277–279°; 94% yield; IR (KBr, cm⁻¹) ν : 3209 (NH), 1667 (C=O), 1275, 1140 (O=S=O); ¹H NMR (700 MHz, DMSO-d₆): δ 11.96 (s, 1H), 8.77 (s, 1H), 8.17 (d, 2H, *J*=8.12 Hz), 8.09 (d, 2H, *J*=8.12 Hz), 7.38 (s, 1H), 6.76 (s, 1H), 3.88 (s, 3H), 3.87 (s, 3H), 3.77 (s, 3H), 3.30 (s, 3H), ¹³C NMR (176 MHz, DMSO-d₆): δ 161.8, 154.0, 152.7, 144.8, 143.7, 143.6, 138.4, 129.0, 127.5, 113.7, 107.9, 98.2, 56.9, 56.3, 56.2, 43.7; C₁₈H₂₀N₂O₆S m/z: 392.1.

4.2. Biological evaluation

4.2.1. In vitro antitumor assay

The antitumor assay was performed for 59 human tumour cell lines obtained from nine human tissue under the protocol of the Drug Evaluation Branch, National Cancer Institute, Bethesda, MD. Three dose-response parameters; GI₅₀, TGI, and LC₅₀; were calculated for each compound^{17,40,70}.

4.2.2. Apoptosis assay

According to our previous report, apoptosis induction was performed using the Leukaemia HL-60 cell line and well-established Annexin 5-FITC/PI detection kit. The cell line samples were analysed using FACSCalibur flow cytometer^{40,72}.

4.2.3. Cell cycle analysis

Cell cycle analysis was carried out similar to our previous report using the Leukaemia HL-60 cell line stained with the DNA fluorochrome PI and analysed by FACSCalibur flow cytometer^{40,74}.

4.2.4. In vitro cyclooxygenase (COX) inhibition assay

The colorimetric COX-2 inhibition assay (kit catalogue number 560101, Cayman Chemical, Ann Arbor, MI) was used to measure the ability of the tested derivatives and celecoxib to inhibit COX-2 isozyme under the manufacturer's instructions^{15,76}.

4.2.5. Egfr and HER2 tyrosine kinases assay

In vitro luminescent EGFR tyrosine kinase assay using Kinase-Glo® MAX as a detection reagent, and *In vitro* HER2 tyrosine kinase assay using DP-Glo™ reagent that measures ADP formed from a kinase reaction, this luminescent signal positively correlates with ADP amount and kinase activity⁴⁰.

4.3. Molecular docking and ADME methodology

Molecular docking protocols were carried out using the MOE 2008.10 software from Chemical Computing Group Inc. (Montreal, QC, Canada) following established methods^{40,81}. The crystal structures of COX-2 (PDB code: 1CX2), EGFR (PDB Code: 1M17), and HER2 (PDB Code: 3PP0) were retrieved from the protein data bank. The Swiss Target Prediction and the Swiss ADME online tools were used to predict the physicochemical, pharmacokinetic, and drug-likeness properties of the test compounds and used reference drugs⁸⁴.

Acknowledgements

The authors thank the Deanship of Scientific Research and RSSU at King Saud University for their technical support.

Disclosure statement

The authors declare that they have no conflict of interest.

Funding

The authors extend their appreciation to the Deanship of Scientific Research at King Saud University for funding this project through the Research Group Project No. RGP-163.

ORCID

Alaa A.-M. Abdel-Aziz  <http://orcid.org/0000-0002-3362-9337>

Adel S. El-Azab  <http://orcid.org/0000-0001-7197-1515>

Nawaf A. AlSaif  <http://orcid.org/0000-0001-9215-1380>

Ahmad J. Obaidullah  <http://orcid.org/0000-0002-7532-6318>

References

1. Avendaño C, Menendez JC. Medicinal chemistry of anti-cancer drugs. Amsterdam, The Netherlands: Elsevier; 2015.
2. Vainshelboim B, Müller J, Lima RM, et al. Cardiorespiratory fitness, physical activity and cancer mortality in men. *Prevent Med* 2017;100:89–94.
3. Varmus H. The new era in cancer research. *Science* 2006; 312:1162–5.
4. Li Q, Xu W. Novel anticancer targets and drug discovery in post genomic age. *Curr Med Chem* 2005;5:53–63.
5. El-Sherbeny MA, Abdel-Aziz AA, Ahmed MA. Synthesis and antitumor evaluation of novel diarylsulfonylurea derivatives: molecular modeling applications. *Euro J Med Chem* 2010;45: 689–97.
6. El-Azab AS, Alanazi AM, Abdel-Aziz NI, et al. Synthesis, molecular modeling study, preliminary antibacterial, and antitumor evaluation of N-substituted naphthalimides and their structural analogues. *Med Chem Res* 2013;22:2360–75.
7. El-Deeb IM, Bayoumi SM, El-Sherbeny MA, Abdel-Aziz AA. Synthesis and antitumor evaluation of novel cyclic arylsulfonylureas: ADME-T and pharmacophore prediction. *Euro J Med Chem* 2010;45:2516–30.
8. Alanazi AM, Abdel-Aziz AA, Shower TZ, et al. Synthesis, antitumor and antimicrobial activity of some new 6-methyl-3-phenyl-4(3H)-quinazolinone analogues: in silico studies. *J Enzyme Inhibition Med Chem* 2016;31:721–35.
9. Alanazi AM, Abdel-Aziz AA, Al-Suwaidan IA, et al. Design, synthesis and biological evaluation of some novel substituted quinazolines as antitumor agents. *Euro J Med Chem* 2014;79:446–54.
10. El-Azab AS, Abdel-Aziz AA, Ghabbour HA, Al-Gendy MA. Synthesis, *in vitro* antitumor activity, and molecular docking study of novel 2-substituted mercapto-3-(3,4,5-trimethoxybenzyl)-4(3H)-quinazolinone analogues. *J Enzyme Inhib Med Chem* 2017;32:1229–39.
11. Mohamed MA, Ayyad RR, Shower TZ, et al. Synthesis and antitumor evaluation of trimethoxyanilides based on 4(3H)-quinazolinone scaffolds. *Euro J Med Chem* 2016;112: 106–13.
12. El-Sayed MA, El-Husseiny WM, Abdel-Aziz NI, et al. Synthesis and biological evaluation of 2-styrylquinolines as antitumor agents and EGFR kinase inhibitors: molecular docking study. *J Enzyme Inhib Med Chem* 2018;33:199–209.
13. Abdel-Aziz AA, El-Azab AS, El-Subbagh HI, et al. Design, synthesis, single-crystal and preliminary antitumor activity of novel arenosulfonylimidazolidin-2-ones. *Bioorg Med Chem Lett* 2012;22:2008–14.
14. Al-Suwaidan IA, Alanazi AM, Abdel-Aziz AA, et al. Design, synthesis and biological evaluation of 2-mercapto-3-phenethylquinazoline bearing anilide fragments as potential antitumor agents: molecular docking study. *Bioorg Med Chem Lett* 2013;23:3935–41.
15. El-Husseiny WM, El-Sayed MA, Abdel-Aziz NI, et al. Structural alterations based on naproxen scaffold: Synthesis, evaluation of antitumor activity and COX-2 inhibition, and molecular docking. *Euro J Med Chem* 2018;158:134–43.
16. Alanazi AM, Al-Suwaidan IA, Alaa A.-M, et al. Design, synthesis and biological evaluation of some novel substituted 2-mercapto-3-phenethylquinazolines as antitumor agents. *Med Chem Res* 2013;22:5566–77.
17. Abdel-Aziz AA, El-Azab AS, Alanazi AM, et al. Synthesis and potential antitumor activity of 7-(4-substituted piperazin-1-yl)-4-oxoquinolines based on ciprofloxacin and norfloxacin scaffolds: in silico studies. *J Enzyme Inhib Med Chem* 2016; 31:796–809.
18. El-Husseiny WM, El-Sayed MA, Abdel-Aziz NI, et al. Synthesis, antitumor and antioxidant activities of novel α,β -unsaturated ketones and related heterocyclic analogues: EGFR inhibition and molecular modelling study. *J Enzyme Inhib Med Chem* 2018;33:507–18.
19. Alanazi AM, El-Azab AS, Al-Suwaidan IA, et al. Synthesis, single-crystal, *in vitro* antitumor evaluation and molecular docking of 3-substituted 5, 5-diphenylimidazolidine-2, 4-dione derivatives. *Medicinal Chemistry Research* 2013;22: 6129–42.
20. Al-Suwaidan IA, Abdel-Aziz AA, Shower TZ, et al. Synthesis, antitumor activity and molecular docking study of some novel 3-benzyl-4(3H)quinazolinone analogues. *J Enzyme Inhib Med Chem* 2016;31:78–89.
21. El-Azab AS, Al-Dhfyhan A, Abdel-Aziz AA, et al. Synthesis, anti-cancer and apoptosis-inducing activities of quinazoline-isatin

- conjugates: epidermal growth factor receptor-tyrosine kinase assay and molecular docking studies. *J Enzyme Inhib Med Chem* 2017;32:935–44.
22. Stratikopoulos EE, Dendy M, Szabolcs M, et al. Kinase and BET Inhibitors Together Clamp Inhibition of PI3K Signaling and Overcome Resistance to Therapy. *Cancer Cell* 2015;27:837–51.
 23. Bayat Mokhtari R, Homayouni TS, Baluch N, et al. Combination therapy in combating cancer. *Oncotarget* 2017;8:38022–43.
 24. Szakács G, Paterson JK, Ludwig JA, et al. Targeting multidrug resistance in cancer. *Nature Reviews. Drug Discovery* 2006;5:219–34.
 25. Fu RG, Sun Y, Sheng WB, Liao DF. Designing multi-targeted agents: An emerging anticancer drug discovery paradigm. *Euro J Med Chem* 2017;136:195–211.
 26. Zhang L, Dewan V, Yin H. Discovery of small molecules as multi-toll-like receptor agonists with proinflammatory and anticancer activities. *J Med Chemistry* 2017;60:5029–44.
 27. Alkahtani HM, Abdalla AN, Obaidullah AJ, et al. Synthesis, cytotoxic evaluation, and molecular docking studies of novel quinazoline derivatives with benzenesulfonamide and anilide tails: Dual inhibitors of EGFR/HER2. *Bioorg Chem* 2020;95:103461.
 28. Daydé-Cazals B, Fauvel B, Singer M, et al. Rational design, synthesis, and biological evaluation of 7-azaindole derivatives as potent focused multi-targeted kinase inhibitors. *J Med Chem* 2016;59:3886–905.
 29. El-Azab AS, Abdel-Aziz AA, Abou-Zeid LA, et al. Synthesis, antitumor activities and molecular docking of thiocarboxylic acid ester-based NSAID scaffolds: COX-2 inhibition and mechanistic studies. *J Enzyme Inhib Med Chem* 2018;33:989–98.
 30. Abdel-Aziz AA, Angeli A, El-Azab AS, et al. Synthesis and anti-inflammatory activity of sulfonamides and carboxylates incorporating trimellitimidates: Dual cyclooxygenase/carbonic anhydrase inhibitory actions. *Bioorg Chem* 2019;84:260–8.
 31. Kolibaba KS, Druker BJ. Protein tyrosine kinases and cancer. *Biochim Biophys Acta* 1997;1333:F217–48.
 32. Antonello A, Tarozzi A, Morroni F, et al. Multitarget-directed drug design strategy: a novel molecule designed to block epidermal growth factor receptor (EGFR) and to exert proapoptotic effects. *J Med Chem* 2006;49:6642–5.
 33. Ishikawa T, Seto M, Banno H, et al. Design and synthesis of novel human epidermal growth factor receptor 2 (HER2)/epidermal growth factor receptor (EGFR) dual inhibitors bearing a pyrrolo[3,2-d]pyrimidine scaffold. *J Med Chem* 2011;54:8030–50.
 34. Salomon DS, Brandt R, Ciardiello F, Normanno N. Epidermal growth factor-related peptides and their receptors in human malignancies. *Crit Rev Oncol Hematol* 1995;19:183–232.
 35. Black JD, Brattain MG, Krishnamurthi SA, et al. ErbB family targeting. *Curr Opin Invest Drugs* 2003;4:1451–4.
 36. Gullick WJ. Prevalence of aberrant expression of the epidermal growth factor receptor in human cancers. *Br Med Bull* 1991;47:87–98.
 37. Woodburn JR. The epidermal growth factor receptor and its inhibition in cancer therapy. *Pharmacol Therapeutics* 1999;82:241–50.
 38. Rusnak DW, Lackey K, Affleck K, et al. The effects of the novel, reversible epidermal growth factor receptor/ErbB-2 tyrosine kinase inhibitor, GW2016, on the growth of human normal and tumor-derived cell lines *in vitro* and *in vivo*. *Mol Cancer Therapeutics* 2001;1:85–94.
 39. Xu G, Abad MC, Connolly PJ, et al. 4-Amino-6-arylamino-pyrimidine-5-carbaldehyde hydrazones as potent ErbB-2/EGFR dual kinase inhibitors. *Bioorganic Med Chem Lett* 2008;18:4615–9.
 40. El-Azab AS, Abdel-Aziz AA, AlSaif NA, et al. Antitumor activity, multitarget mechanisms, and molecular docking studies of quinazoline derivatives based on a benzenesulfonamide scaffold: Cell cycle analysis. *Bioorg Chem* 2020;104:104345.
 41. Alkahtani HM, Alanazi MM, Aleanizy FS, et al. Synthesis, anticancer, apoptosis-inducing activities and EGFR and VEGFR2 assay mechanistic studies of 5,5-diphenylimidazolidine-2,4-dione derivatives: Molecular docking studies. *Saudi Pharmaceutical J* 2019;27:682–93.
 42. Gundla R, Kazemi R, Sanam R, et al. Discovery of novel small-molecule inhibitors of human epidermal growth factor receptor-2: combined ligand and target-based approach. *J Med Chem* 2008;51:3367–77.
 43. Danchev N, Nikolova I, Momekov G. A new era in anticancer therapy/imatinib—a new era in anticancer therapy. *Biotechnol Biotechnol Equip.* 2008;22(3):769–70.
 44. Iqbal N, Iqbal N. Imatinib: a breakthrough of targeted therapy in cancer. *Chemother Res Pract.* 2014;2014:1–9.
 45. Madhusudan S, Ganesan TS. Tyrosine kinase inhibitors in cancer therapy. *Clin Biochem.* 2004;37:618–35.
 46. Barker AJ, Gibson KH, Grundy W, et al. Studies leading to the identification of ZD1839 (IressaTM): an orally active, selective epidermal growth factor receptor tyrosine kinase inhibitor targeted to the treatment of cancer. *Bioorg Med Chem Lett.* 2001;11:1911–4.
 47. Frampton JE. Lapatinib: a review of its use in the treatment of HER2-overexpressing, trastuzumab-refractory, advanced or metastatic breast cancer. *Drugs* 2009;69:2125–48.
 48. Takimoto CH, Awada A. Safety and anti-tumor activity of sorafenib (Nexavar) in combination with other anti-cancer agents: a review of clinical trials. *Cancer Chemother Pharmacol.* 2008;61:535–48.
 49. Dungo RT, Keating GM. Afatinib: first global approval. *Drugs* 2013;73:1503–15.
 50. Christensen JG. A preclinical review of sunitinib, a multitargeted receptor tyrosine kinase inhibitor with anti-angiogenic and antitumor activities. *Ann Oncol* 2007;18: x3–10.
 51. Ghosh N, Chaki R, Mandal V, Mandal SC. COX-2 as a target for cancer chemotherapy. *Pharmacol Rep PR* 2010;62:233–44.
 52. Blanke C. Role of COX-2 inhibitors in cancer therapy. *Cancer Invest* 2004;22:271–82.
 53. Dai ZJ, Ma XB, Kang HF, et al. Antitumor activity of the selective cyclooxygenase-2 inhibitor, celecoxib, on breast cancer *in Vitro* and *in Vivo*. *Cancer Cell Inter* 2012;12:53.
 54. Vosooghi M, Amini M. The discovery and development of cyclooxygenase-2 inhibitors as potential anticancer therapies. *Exp Opin Drug Disc* 2014;9:255–67.
 55. Elder DJ, Halton DE, Hague A, Paraskeva C. Induction of apoptotic cell death in human colorectal carcinoma cell lines by a cyclooxygenase-2 (COX-2)-selective nonsteroidal anti-inflammatory drug: independence from COX-2 protein expression. *Clin Cancer Res* 1997;3:1679–83.
 56. Hodnett EM, Dunn WJ. 3rd., Structure-antitumor activity correlation of some Schiff bases. *J Med Chem* 1970;13:768–70.
 57. Petrović ZD, Dorović J, Simijonović D, et al. Experimental and theoretical study of antioxidative properties of some

- salicylaldehyde and vanillic Schiff bases. *RSC Advances* 2015; 5:24094–100.
58. el-Ayaan U, Abdel-Aziz AA. Synthesis, antimicrobial activity and molecular modeling of cobalt and nickel complexes containing the bulky ligand: bis[N-(2,6-diisopropylphenyl)imino]acenaphthene. *Euro J Med Chem* 2005;40:1214–21.
 59. Zineddine Z, Suat T, Hasan K, et al. Synthesis and anti-cancer properties of novel hydrazone derivatives incorporating pyridine and isatin moieties. *Arch Pharm* 2020;354: e2000377.
 60. Vogel S, Kaufmann D, Pojarová M, et al. Aroyl hydrazones of 2-phenylindole-3-carbaldehydes as novel antimetabolic agents. *Bioorg Med Chem* 2008;16:6436–47.
 61. Rollas S, Küçükgül SG. Biological activities of hydrazone derivatives. *Molecules* 2007;12:1910–39.
 62. Liang Z, Zhang D, Ai J, et al. Identification and synthesis of N'-(2-oxindolin-3-ylidene)hydrazide derivatives against c-Met kinase. *Bioorg Med Chem Lett* 2011;21:3749–54.
 63. Peterson QP, Hsu DC, Goode DR, et al. Procaspace-3 activation as an anti-cancer strategy: Structure – activity relationship of procaspase-activating compound 1 (PAC-1) and its cellular co-localization with caspase-3. *J Med Chem* 2009;52: 5721–31.
 64. Abdel-Aziz AA, El-Azab AS, Abu El-Enin MA, et al. Synthesis of novel isoindoline-1,3-dione-based oximes and benzene-sulfonamide hydrazones as selective inhibitors of the tumor-associated carbonic anhydrase IX. *Bioorg Chem* 2018;80: 706–13.
 65. El-Azab AS, Abdel-Aziz AA, Bua S, et al. Synthesis and comparative carbonic anhydrase inhibition of new Schiff's bases incorporating benzenesulfonamide, methanesulfonamide, and methylsulfonylbenzene scaffolds. *Bioorg Chem* 2019;92: 103225.
 66. Şenkardeş S, Han M, Kulabaş N, et al. Synthesis, molecular docking and evaluation of novel sulfonyl hydrazones as anti-cancer agents and COX-2 inhibitors. *Mol Diversity* 2020;24: 673–89.
 67. Bánvölgyi A, Anker P, Lőrincz K, et al. Smoothed receptor inhibitor vismodegib for the treatment of basal cell carcinoma: a retrospective analysis of efficacy and side effects. *J Dermatol Treat* 2020;31:387–98.
 68. Gould SE, Low JA, Marsters JC, Jr, et al. Discovery and pre-clinical development of vismodegib. *Exp Opin Drug Disc* 2014;9:969–84.
 69. George RF. Facile synthesis of simple 2-oxindole-based compounds with promising antiproliferative activity. *Fut Med Chem* 2018;10:269–82.
 70. Shoemaker RH. The NCI60 human tumour cell line anti-cancer drug screen. *Nat Rev Cancer* 2006;6:813–23.
 71. Pfeffer CM, Singh AT. Apoptosis: a target for anticancer therapy. *Inter J Mol Sci* 2018;19:448.
 72. Vermes I, Haanen C, Steffens-Nakken H, Reutelingsperger C. A novel assay for apoptosis flow cytometric detection of phosphatidylserine expression on early apoptotic cells using fluorescein labelled annexin V. *J Immunol Methods* 1995; 184:39–51.
 73. Ormerod MG. Investigating the relationship between the cell cycle and apoptosis using flow cytometry. *J Immunol Methods* 2002;265:73–80.
 74. Kim KH, Sederstrom JM. Assaying cell cycle status using flow cytometry. *Curr Protoc Mol Biol* 2015;111:28.6. 1–6. 11.
 75. Gurpinar E, Grizzle WE, Piazza GA. COX-Independent mechanisms of cancer chemoprevention by anti-inflammatory drugs. *Front Oncol* 2013;3:181.
 76. Abdel-Aziz AA, El-Azab AS, Abou-Zeid LA, et al. Synthesis, anti-inflammatory, analgesic and COX-1/2 inhibition activities of anilides based on 5,5-diphenylimidazolidine-2,4-dione scaffold: Molecular docking studies. *Euro J Med Chem* 2016;115:121–31.
 77. Abdel-Aziz AA, Asiri YA, Al-Agamy MH. Design, synthesis and antibacterial activity of fluoroquinolones containing bulky arenesulfonyl fragment: 2D-QSAR and docking study. *Euro J Med Chem* 2011;46:5487–97.
 78. Goda FE, Abdel-Aziz AA, Ghoneim HA. Synthesis and biological evaluation of novel 6-nitro-5-substituted aminoquinolines as local anesthetic and anti-arrhythmic agents: molecular modeling study. *Bioorg Med Chem* 2005;13: 3175–83.
 79. El-Azab AS, Mary YS, Panicker CY, et al. DFT and experimental (FT-IR and FT-Raman) investigation of vibrational spectroscopy and molecular docking studies of 2-(4-oxo-3-phenethyl-3, 4-dihydroquinazolin-2-ylthio)-N-(3, 4, 5-trimethoxyphenyl) acetamide. *J Mol Struct* 2016;1113:133–45.
 80. El-Gamal MI, Bayomi SM, El-Ashry SM, et al. Synthesis and anti-inflammatory activity of novel (substituted)benzylidene acetone oxime ether derivatives: molecular modeling study. *Euro J Med Chem* 2010;45:1403–14.
 81. MOE 2008.10 of Chemical Computing Group. Inc. Available from: http://www.chemcomp.com/press_releases/2008-11-04.htm.
 82. Abdel-Aziz AA, Abou-Zeid LA, ElTahir KE, et al. Design, synthesis of 2,3-disubstitued 4(3H)-quinazolinone derivatives as anti-inflammatory and analgesic agents: COX-1/2 inhibitory activities and molecular docking studies. *Bioorg Med Chem* 2016;24:3818–28.
 83. Abdel-Sayed MA, Bayomi SM, El-Sherbeny MA, et al. Synthesis, anti-inflammatory, analgesic, COX-1/2 inhibition activities and molecular docking study of pyrazoline derivatives. *Bioorg Med Chem* 2016;24:2032–42.
 84. Swiss Institute of Bioinformatics. <http://www.swissadme.ch/index.php>.
 85. Lipinski CA, Lombardo F, Dominy BW, Feeney PJ. Experimental and computational approaches to estimate solubility and permeability in drug discovery and development settings. *Adv Drug Del Rev* 2001;46:3–26.
 86. Veber DF, Johnson SR, Cheng HY, et al. Molecular properties that influence the oral bioavailability of drug candidates. *J Med Chem* 2002;45:2615–23.
 87. Egan WJ, Merz KM, Jr., Baldwin JJ. Prediction of drug absorption using multivariate statistics. *J Med Chem* 2000; 43:3867–77.
 88. Daina A, Zoete V. A BOILED-Egg To Predict Gastrointestinal Absorption and Brain Penetration of Small Molecules. *Chem Med Chem* 2016;11:1117–21.
 89. Daina A, Michielin O, Zoete V. SwissADME: a free web tool to evaluate pharmacokinetics, drug-likeness and medicinal chemistry friendliness of small molecules. *Sci Rep* 2017;7:42717.
 90. Szakács G, Váradi A, Ozvegy-Laczkó C, Sarkadi B. The role of ABC transporters in drug absorption, distribution, metabolism, excretion and toxicity (ADME-Tox). *Drug Disc Today* 2008;13:379–93.
 91. Daina A, Michielin O, Zoete V. iLOGP: a simple, robust, and efficient description of n-octanol/water partition coefficient for drug design using the GB/SA approach. *J Chem Inform Model* 2014;54:3284–301.